Best
Available
Copy

AD-A282 018

June 20, 1994 Reprint

STATISTICAL PROPERTIES OF SOLAR GRANULATION DERIVED FROM THE SOUP INSTRUMENT ON SPACELAB 2

PE 61102F
PR 2311
TA G3
WU 27

A.M.Title*, T.D.Tarbell*, K.P.Topka*, S.H.Ferguson*, R.A. Shine*, and the SOUP Team[1]

Phillips Lab/GPSS
29 Randolph Road
Hanscom AFB, MA 01731-3010

PL-TR-94-2175

DTIC
ELECTE
JUN 29 1994
S B D

*Lockheed Palo Alto Research Laboratory

[1] L. Acton, D. Duncan, M. Finch, Z. Frank, G. Kelly, R. Lindgren, M. Morrill, N. Ogle (deceased), T. Pope, R. Reeves, R. Rehse, and R. Wallace, Lockheed Palo Alto Research Laboratory; J. Harvey, J. Leibacher, W. Livingston, L. November, and H. Ramsey, National Solar Observatory; G. Simon, Air Force Geophysics Laboratory.

Reprinted from Astrophysical Journal 336: 475-494, 1989 January 1

Approved for public release; distribution unlimited

The Solar Optical Universal Polarimeter (SOUP) on Spacelab 2 collected movies of solar granulation completely free from the distortion and blurring introduced by the Earth's atmosphere. Individual images in the movies are diffraction-limited (30 cm aperture) and are not degraded by pointing jitter (the pointing stability was 0".003 root mean square). The movies illustrate that the solar 5 minute oscillation has a major role in the appearance of solar granulation and that exploding granules are a common feature of the granule evolution. Using three-dimensional Fourier filtering techniques, we have been able to remove the oscillations and demonstrate that they dominate the temporal autocorrelation functions of the granulation pattern. When the oscillations are removed, the autocorrelation lifetime of granulation is a factor of 2 greater in magnetic field regions than in field-free quiet Sun. Using a technique called local correlation tracking, we have been able to measure horizontal velocities and observe flow patterns on the scale of meso- and supergranulation. In quiet regions the mean flow velocity is 370 m s^{-1}, while in magnetic regions it is about 125 m s^{-1}. We have also found that the root mean square fluctuating horizontal velocity field in quiet Sun increases from 0.45 to 1.4 km s^{-1}, and in strong magnetic field regions it increases from 0.3 to 0.75 km s^{-1} as the measuring aperture decreases from 4" to 1". Combining the results from temporal and spatial autocorrelation functions with the velocity measurements, we conclude that the decay of the temporal autocorrelation function is due as much to motion and distortion of granules as to lifetimes of elements in the pattern. Attempts to follow granules using image-processing techniques yields a lifetime for individual features on the order of 5 minutes. The size distribution, lifetime, and proper motions are also derived and compared with the measurements. By superposing the location of exploding granules on the average flow maps, we find that they appear almost exclusively in the center of mesogranulation size flow cells. The density of exploding granules is sufficient for their expansion fronts to cover a typical mesogranule in 900 s. Because of the nonuniformity of the distribution of exploding granules, the evolution of the granulation pattern in mesogranule cell centers differs fundamentally from that in boundaries. It is clear from this study that there is neither a typical granule nor a typical granule evolution. Even after the solar oscillations are removed, a granule's evolution is dependent on local magnetic flux density, its position with respect to the active region plage, its position in the mesogranulation pattern, and evolution of granules in its immediate neighborhood.

14. SUBJECT TERMS			NUMBER OF PAGES
Granulation, Mesogranulation, Sun: Atmospheric motions, Sun: Oscillation			20
			16. PRICE CODE
17. SECURITY CLASSIFICATION OF REPORT	18. SECURITY CLASSIFICATION OF THIS PAGE	19. SECURITY CLASSIFICATION OF ABSTRACT	20. LIMITATION OF ABSTRACT
UNCLASSIFIED	UNCLASSIFIED	UNCLASSIFIED	SAR

NSN 7540-01-280-5500

DTIC QUALITY INSPECTED 1

Standard Form 298 (Rev. 2-89)
Prescribed by ANSI Std. Z39-18
298-102

PL-TR-94-2175

THE ASTROPHYSICAL JOURNAL, 336:475–494, 1989 January 1
© 1989 The American Astronomical Society. All rights reserved. Printed in U.S.A.

STATISTICAL PROPERTIES OF SOLAR GRANULATION DERIVED FROM THE SOUP INSTRUMENT ON SPACELAB 2

A. M. TITLE, T. D. TARBELL, K. P. TOPKA, S. H. FERGUSON, AND R. A. SHINE
Lockheed Palo Alto Research Laboratory

AND

THE SOUP TEAM[1]

Received 1988 March 24; accepted 1988 June 14

ABSTRACT

The Solar Optical Universal Polarimeter (SOUP) on Spacelab 2 collected movies of solar granulation completely free from the distortion and blurring introduced by the Earth's atmosphere. Individual images in the movies are diffraction-limited (30 cm aperture) and are not degraded by pointing jitter (the pointing stability was 0".003 root mean square). The movies illustrate that the solar 5 minute oscillation has a major role in the appearance of solar granulation and that exploding granules are a common feature of the granule evolution. Using three-dimensional Fourier filtering techniques, we have been able to remove the oscillations and demonstrate that they dominate the temporal autocorrelation functions of the granulation pattern. When the oscillations are removed, the autocorrelation lifetime of granulation is a factor of 2 greater in magnetic field regions than in field-free quiet Sun. Using a technique called local correlation tracking, we have been able to measure horizontal velocities and observe flow patterns on the scale of meso- and supergranulation. In quiet regions the mean flow velocity is 370 m s^{-1}, while in magnetic regions it is about 125 m s^{-1}. We have also found that the root mean square fluctuating horizontal velocity field in quiet Sun increases from 0.45 to 1.4 km s^{-1}, and in strong magnetic field regions it increases from 0.3 to 0.75 km s^{-1} as the measuring aperture decreases from 4" to 1". Combining the results from temporal and spatial autocorrelation functions with the velocity measurements, we conclude that the decay of the temporal autocorrelation function is due as much to motion and distortion of granules as to lifetimes of elements in the pattern. Attempts to follow granules using image-processing techniques yields a lifetime for individual features on the order of 5 minutes. The size distribution, lifetime, and proper motions are also derived and compared with the measurements. By superposing the location of exploding granules on the average flow maps, we find that they appear almost exclusively in the center of mesogranulation size flow cells. The density of exploding granules is sufficient for their expansion fronts to cover a typical mesogranule in 900 s. Because of the nonuniformity of the distribution of exploding granules, the evolution of the granulation pattern in mesogranule cell centers differs fundamentally from that in boundaries. It is clear from this study that there is neither a typical granule nor a typical granule evolution. Even after the solar oscillations are removed, a granule's evolution is dependent on local magnetic flux density, its position with respect to the active region plage, its position in the mesogranulation pattern, and evolution of granules in its immediate neighborhood.

Subject headings: Sun: atmospheric motions — Sun: granulation — Sun: oscillations

I. INTRODUCTION

In recent years there have been excellent reviews of granulation by Wittmann (1979), Beckers (1981), and Bray, Loughhead, and Durrant (1984). However, a number of what are thought to be significant properties of the granulation, for example, lifetime, size, and evolution (Kitai and Kawaguchi 1979; Oda 1984; Kawaguchi 1980; Roudier and Muller 1987), are still under active discussion. Although the majority of astronomers believe that granules are thermal plumes overshooting from the convection zone into the photosphere (Bray, Loughhead, and Durrant 1984; Nordlund 1985), there is some evidence that they are turbulent eddies (Zahn 1987). The relative contribution of wave and convective motion to the velocity field of the photosphere is still controversial (Beckers 1981; Nordlund 1985; Cox 1988). At present it is not possible to answer the question, "What is a typical granule?" In view of the current status it is not surprising that there exists no better discussion of granule time histories than that given by Mehltretter (1978), which was based on images from the Spektrostratoskop balloon flight of 1975.

In our opinion there are four primary reasons for the current difficulties: a limited number of good time sequences of granulation images, a lack of good repeatable definitions for physical properties in an evolving flow pattern, limitations on storage capacity and computational power of previous computer image processing systems for handling high-resolution time sequences, and a shortage of high-resolution numerical simulations of granulation.

Although quality granulation photographs have been obtained for nearly a century (Janssen 1896), until recently there were very few time sequences of high uniform quality. The Stratoscope, Spektrostratoskop, and Soviet Stratoscopic Observatory balloon programs represent the main data base for the reported investigations of granule evolution. While

[1] L. Acton, D. Duncan, M. Finch, Z. Frank, G. Kelly, R. Lindgren, M. Morrill, N. Ogle (deceased), T. Pope, R. Reeves, R. Rehse, and R. Wallace, Lockheed Palo Alto Research Laboratory; J. Harvey, J. Leibacher, W. Livingston, L. November, and H. Ramsey, National Solar Observatory; G. Simon, Air Force Geophysics Laboratory.

94-19540

94 6 27 021

these telescopes produced many excellent images in quiet Sun, problems with focus shift and pointing stability compromised their time sequences. Because of the variations in quality and pointing, studies of these data have depended largely on sets of photographs rather than movies. Ground-based observatories, in particular Pic du Midi, have produced truly outstanding images, but again movies are rare. In the past year both the Big Bear Solar Observatory and the Swedish Observatory on La Palma have produced some good to outstanding movies, and computer-intensive analyses based on the techniques developed for handling SOUP movies are now underway.

The lack of good movies has aggravated objectively defining a granule and granule evolution. The traditional statistical tools for characterizing intensity fluctuations in the photosphere sidestep this problem. Unfortunately, they also include other physical processes and instrumental effects unrelated to granules. Spatial autocorrelation functions (ACFs) and their Fourier transforms, and intensity power spectra, are all compromised by lack of knowledge of the combined modulation transfer function of the atmosphere, telescope, and detector system (Bahng and Schwarzschild 1962; Schmidt, Knolker, and Schroter 1981; Nordlund 1984). The SOUP data are only partially free of these problems. Temporal ACFs do not separate decorrelations due to size and shape changes from proper motions, nor do they distinguish changes due to the convective flows from other patterns, such as oscillations and waves.

Another class of techniques use pattern recognition algorithms to locate granules, identify the same granule at different times, and derive various properties of the set of granules selected. We have found that each algorithm has its own peculiar sensitivities, and it is very difficult to get consistent results from different algorithms. For example, attempts to isolate granules by thresholding techniques are sensitive to small- and large-scale intensity variations introduced by wave patterns. Most granule identification processes ultimately are based on subjective criteria of the observer. Because these criteria are not universal or even well defined, it is very difficult to compare observations of different groups, or to have a great deal of confidence in solar cycle variations of granulation parameters, unless a single group has reduced all the observations.

The study of solar images using modern image processing systems requires large amounts of storage capacity. Good granulation images have a resolution of 0".5 or better. If three samples are taken per resolution element, each 10" square region of the Sun implies a 60 × 60 array, or 3600 pixels. A region large enough to include a supergranule, 40", needs a 240 × 240 array. For convenience 256 × 256 pixel arrays are usually studied, and this requires between 64 and 128 kilobytes of computer memory. A time sequence of 0.5 hr with 10 s time resolution requires between 12 and 24 megabytes of memory. Fourier transform operations typically require 4–8 byte precision for the data. Thus performing three-dimensional Fourier transforms involves data blocks of several hundred megabytes. Until recently, computing capabilities on this order have not been generally available for the reduction of solar data; of course, better resolution compounds these problems.

Because of the difficulties in defining flow patterns and the computational effort required to identify any order in a movie, the solar observer may be greatly aided by good theoretical guidance. Unfortunately, three-dimensional modeling is expensive. Currently 32 × 32 × 32 volumes can be examined, which are really not large enough to understand the granule-granule interactions caused by the larger scale flows of meso- and supergranulation and by wave generation. It is to be hoped that the 64 × 64 × 64 volumes now being used for these calculations will provide more guidance. Nonetheless, the computational simulations of Dravins, Lindegren, and Nordlund (1981), Nordlund (1985), Steffen, Ludwig, and Kruss (1988), and Hurlburt, Toomre, and Massaguer (1984, 1986) clearly have many of the features seen in solar images.

The flight of SOUP on Spacelab 2 (Title *et al.* 1986) produced nearly 6000 good granulation images, but, much more important, it produced several movies of almost 30 minutes in length. These movies are essentially diffraction-limited (30 cm aperture) and are free of frame-to-frame changes in image quality and pointing jitter (0".003 root mean square [rms]). The movies are qualitatively different from any previous ground-based movies. From the first viewings, it was clear that oscillations played a major role in the appearance of the photospheric surface, that exploding granules were much more common than have previously been suggested (Title *et al.* 1987), that there were regions of ordered flow (November *et al.* 1987), and that magnetic fields affected the time history of granulation (Simon *et al.* 1988).

The SOUP team was prepared to handle the massive data reduction task required for movies. An analog laser disk system was developed for interactive display of movies and movie sequences. A large amount of digital magnetic and laser disk capacity was available for the immediate and final data products. Interactive image-processing tools suitable for handling large sets of images were in place, and a small staff was available for the digitization of the images and the management of tapes and disk storage space.

Because of the analysis capacity we have been able to apply a number of image-processing algorithms for the characterization of granulation. In particular, three-dimensional Fourier filtering to remove solar oscillations has been possible. In § III we show that solar oscillations dominate the temporal ACFs. When these oscillations are removed, it is clear that quiet and magnetic regions differ significantly in temporal history. The differences between quiet and magnetic Sun are also visible in their average intensities and their rms intensity fluctuations (§ IV) and quasi-steady horizontal velocities (§ V). The more accurate estimate of the ACF lifetime obtained from Fourier filtered images coupled with horizontal velocities obtained by local correlation tracking lead us to suggest in § V that the temporal change in the ACF is dominated by displacements rather than lifetime of the individual granules.

The traditional technique of determining lifetimes is to identify granules and then track them from beginning to end. In § VI this has been done automatically with two different identification algorithms. These automatic procedures yield lifetimes that are much shorter than might be expected from the temporal ACF. This result probably is caused by the fact that granules have internal structure—multiple bright points and dark lanes—which changes during their evolution. We have also measured granule densities, sizes, velocities, and spacings, and the distribution functions of these properties. Our results bracket measurements found previously. The range in granule properties found by different algorithms shows that granule characteristics are strongly dependent on the process used to define them.

In § VII we discuss exploding granules. In the SOUP data at least half the solar surface is affected by the circle of expansion of an exploding granule. Often, a granule is terminated (e.g.,

squashed) by a neighboring exploder. Further, these exploders are concentrated in meso- and supergranule interiors, so that their effects are not uniform. Because of this fundamental nonuniform distribution, lifetimes of individual granules are often determined by events in their local neighborhood, which in turn depends on their position in the mesogranulation pattern.

Finally, in § VIII, we summarize our results and stress that there is not a single "typical" granulation evolution pattern. Rather, the surface of the Sun has brightness fluctuations which are caused by a combination of convection, turbulence, waves, and magnetic fields. It is impossible to separate these effects in a single image, and the first steps in effecting the separation in movie data are reported here. The evolutionary history of a bright feature on the surface of the Sun depends on where it is born in a preexisting flow field, how close it is to an exploding granule, and how much magnetic flux is in its vicinity.

II. OBSERVATIONS

The granulation data were all collected on Kodak SO 253 film using the SOUP instrument during the flight of Spacelab 2 (Title *et al.*, 1986). The original images are 140″ × 250″ and are taken in a thousand angstrom band centered at 6000 Å. The images are very uniform in quality and are distortion-free. Using the Spacelab Instrument Pointing System and an internal fast guider, image stability of 0″.003 rms was achieved during quiescent periods, and peak disturbances were less than 0″.03.

The original film was digitized using a 1024 × 1024 CCD camera developed for the High Resolution Solar Observatory program of NASA. The film was mounted in a high-precision animation projector with a double integrating sphere light source and imaged onto the CCD using a high-quality copying lens mounted on a x-y-z stage. By moving the lens and stage, any section and magnification of the film frame could be selected for digitizing. The 12 bit digital images were transferred directly to the Lockheed Palo Alto Research Laboratory VAX 780 for processing and analysis. The raw digital images were corrected for both flat field and dark current. Solar rotation and slow drift of the pointing were measured by cross-correlating consecutive images in a movie. These effects were then removed by shifting images rigidly using bicubic interpolation. A more detailed discussion of the analysis process is contained in Simon *et al.* (1988).

For this report we have studied four digitized subsections, two quiet Sun regions (34″ × 34″ and 40″ × 40″), and two regions centered on the pores (34″ × 34″ and 60″ × 60″). The pores are part of AR 4682 at approximately S15, W31 ($\mu = 0.75$). Because of limitations of the processing computer and our image display system, all digital images are 256 × 256 pixels. This implies 0″.134 and 0″.161 pixels for the quiet Sun regions, and 0″.134 and 0″.234 pixels for the pore region, respectively. The film frames were separated by 2 s in time and cover 1650 s. The results reported here are all from orbit 110 (19:10:35 to 19:38:07 GMT on 1985 August 5). For most of the results reported here we have used data with 10 or 20 s time separations.

In addition, we have used magnetograms collected at the Big Bear Solar Observatory (BBSO) during orbit 110. The BBSO magnetograms were supplied in digital form on magnetic tape. They were rescaled, rotated, and rectified, so that the SOUP and BBSO images could be accurately coaligned.

III. TEMPORAL AUTOCORRELATION MEASUREMENTS

We define the correlation lifetime of granulation by the $1/e$ width of temporal ACF, where the temporal ACF of the intensity is defined as

$$\mathrm{ACF}(\tau) = \frac{\langle \delta I(x, y, t_0)\delta I(x, y, t_0 + \tau)\rangle}{\langle \delta I^2(x, y, t_0)\rangle},$$

where x and y are the spatial coordinates, t_0 is the time, and τ is the time separation. The brackets indicate an average over space and time, and

$$\delta I(x, y, t) = I(x, y, t) - \langle I(x, y, t)\rangle .$$

The ACF has been calculated for granulation in quiet Sun regions essentially free of strong magnetic fields and in the magnetic field regions in the vicinity of the active region. The locations of quiet and magnetic areas were determined with the BBSO magnetograms by carefully registering features visible on both the SOUP and the BBSO images, namely, the sunspot and pores. After superposition, isogauss contours from the magnetogram were overlaid onto the SOUP images using our image display system. Small image areas (24 × 24 pixels, called "boxes") were then chosen to be either outside (quiet Sun) or inside (magnetic areas) of the contours. The sunspots and pores were avoided. Results for larger areas were obtained by averaging ACFs from several boxes.

Four image sequences were used, comprising three different fields of view. This allowed us to compare our results from different areas of the Sun at different image scales, and also allowed comparison of quiet Sun and magnetic areas at the same image scale. Figure 1 (Plate 10) shows a quiet Sun image (*top*) and a pore region image (*bottom*). Indicated on both are the sample boxes used to calculate the ACFs and the BBSO magnetogram contours.

The ACFs from the quiet Sun sequences are shown in Figure 2. These results are the average of 16 boxes for the 0″.161 pixel^{-1} sequence (*solid line*) and the entire field of view for the 0″.134 pixel^{-1} sequence (*dashed line*). The 24 × 24 pixel boxes were used in the former case because it contains regions with significant magnetic flux, which were avoided. The quiet Sun correlation lifetime is about 5 minutes. Measurements from a number of other studies (Mehltretter 1978) are also included in Figure 2. Previous ACF lifetime measurements of granulation have ranged from 3 to 7 minutes, with an average of about 6 minutes (Wittmann 1979). As can be seen from the figure, both the shape of the ACFs and the determined lifetime of the SOUP data are in agreement with the previous values.

The ACFs from the individual boxes indicated in Figure 1, which cover only 36 arcsec^2, are qualitatively different from their sum. Figure 3 (*solid curves*) shows the ACFs generated from four of these boxes in regions of quiet Sun. These ACFs do not drop monotonically, but rather exhibit oscillations with periods of 3–6 minutes (depending on the sample). This suggests that solar oscillations are affecting the correlation lifetime, which is not too surprising, since they are strongly visible in the granulation movies.

The average ACF over a sufficiently large region does not oscillate as strongly as a small region. This is exhibited in Figure 4, which shows a three-dimensional isometric ACF plot: correlation coefficient versus time lag and area. To create the figure, we have calculated ACFs from a nested sequence of square regions varying from 12 to 400 arcsec^2. As the area of the Sun used for the ACF measurement increases, the oscillations decrease.

Codes
Avail and/or
Dist Special
A-1 20

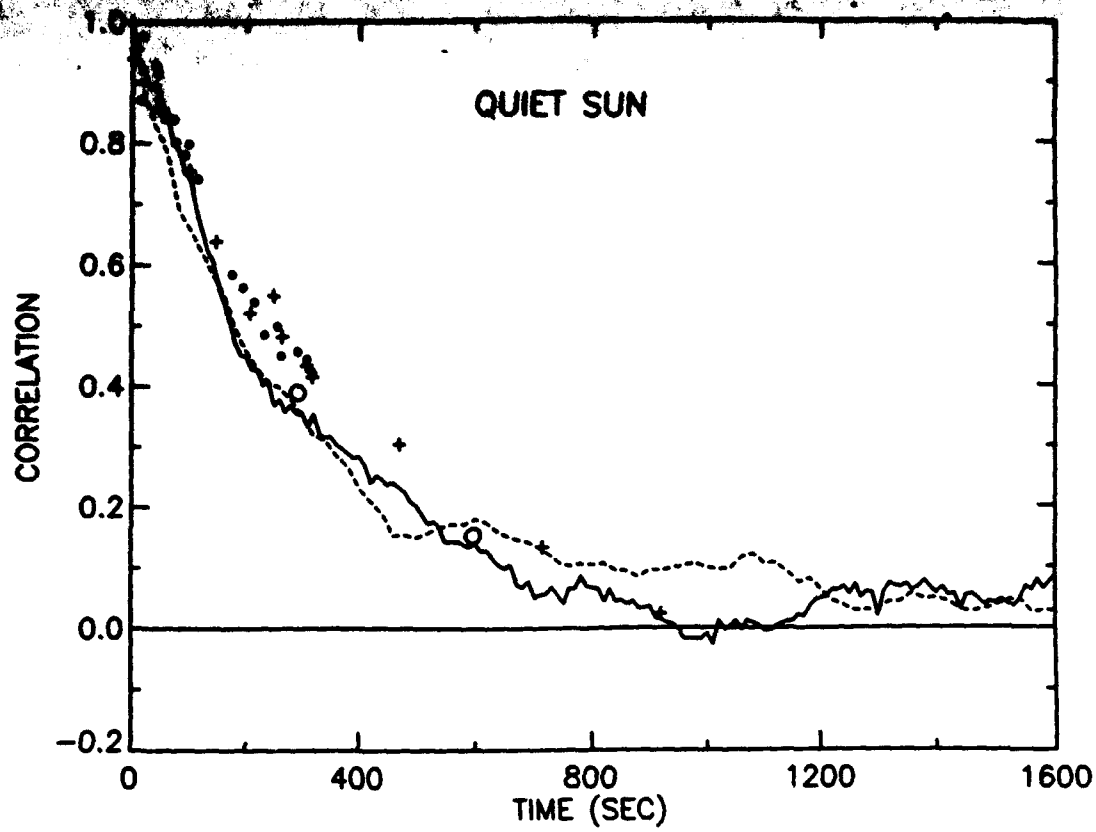

FIG. 2.—Autocorrelation functions from two quiet Sun regions, original data. *Solid line*: 0".161 pixel^{-1} image sequence; *dashed line*: 0".134 pixel^{-1} image sequence. Superposed are autocorrelation measurements from previously published results for comparison (*dots, crosses, open circles*).

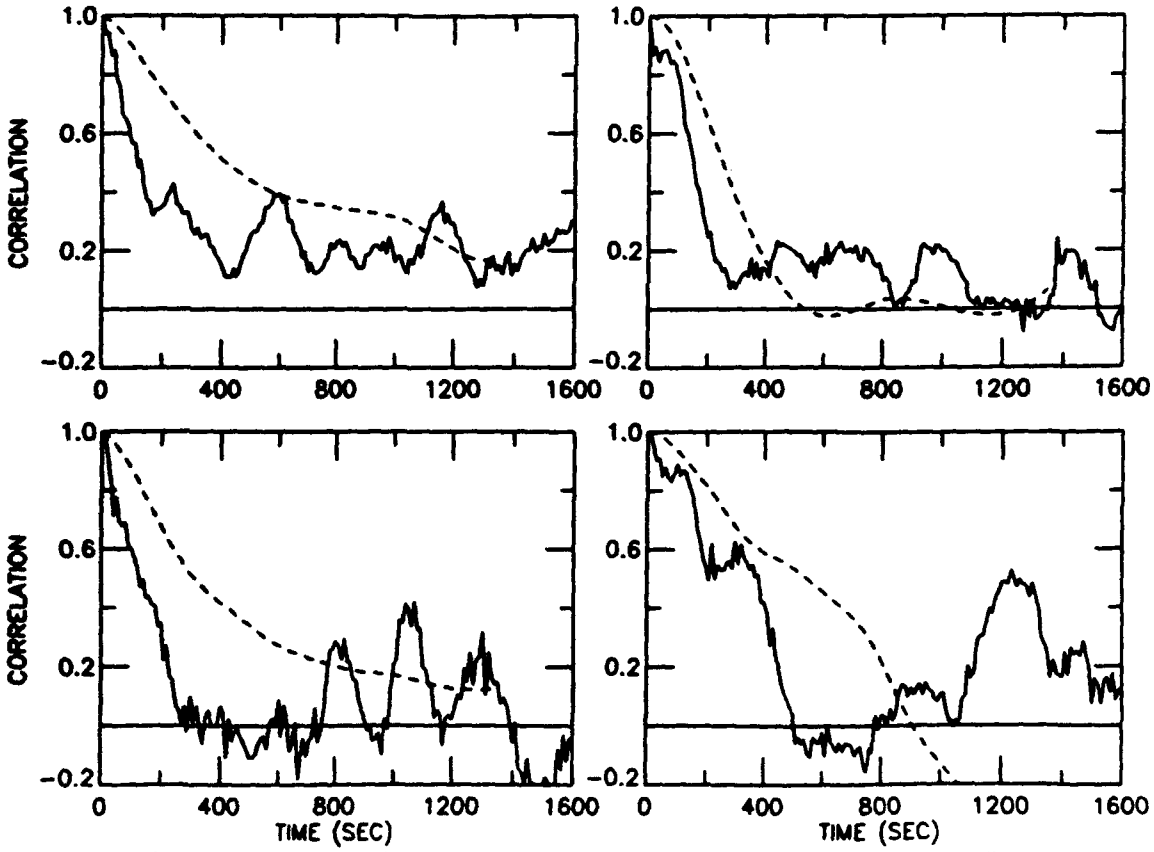

FIG. 3.—Autocorrelation functions in 6" × 6" boxes of quiet Sun from an original image sequence (*solid curves*), showing the effects of intensity oscillations. The dashed curves are from the same four boxes after three-dimensional Fourier filtering of the image sequence to remove the effects of oscillations.

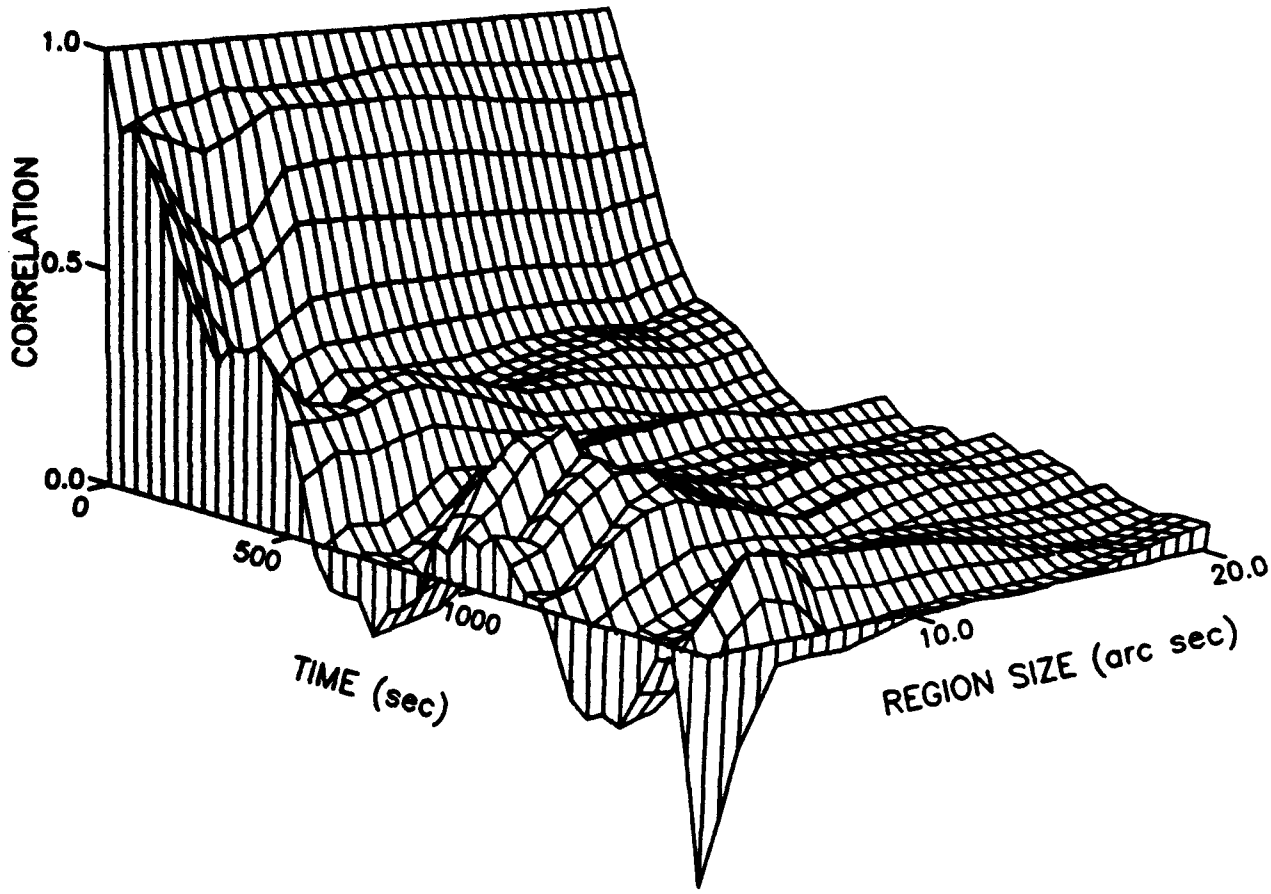

FIG. 4.—Autocorrelation function in quiet Sun plotted as a three-dimensional surface, illustrating how oscillations tend to dampen with increasing region size. The x-axis is time, the y-axis is region size, and the z-axis is correlation amplitude.

To remove the effect of oscillations, we have applied what we call a subsonic Fourier filter. A raw image sequence, which can be considered to be a single three-dimensional function of intensity (I_x, I_y) and time (t), is Fourier transformed into a function of k_x, k_y, and ω. The subsonic filter is defined by a cone,

$$v_p = \frac{\omega}{k},$$

in (k, ω)-space, where k and ω are spatial and temporal frequencies and v_p is the maximum phase velocity. All Fourier components inside the cone (i.e., with phase velocities less than v_p) are retained, while all those outside are set to zero. Then a new sequence of images is calculated by an inverse Fourier transform. For the subsonic filters, values of v_p of 3, 4, and 5 km s^{-1}, well below the 7 km s^{-1} sound speed, were used. For these values of v_p, the velocity cone is totally inside the region occupied by the solar f- and p-modes.

A subsonic filtered movie exhibits very little solar oscillation, and the same is true of the ACFs formed from subsonic filtered data. The dashed curves in Figure 3 are made from the same areas as the solid curves but are from subsonic filtered (v_p = 3 km s^{-1}) rather than original data. Figure 5 shows a comparison of the ACFs from 300 arcsec^2 of quiet Sun for (a) the original data and (b) the subsonic filtered image sequences. The quiet Sun ACF lifetime of the subsonic data is 1.5 times greater than the original—a lifetime of 410 versus 270 s.

We have investigated the effects of our choice of subsonic filter, and whether an abrupt cutoff had any important consequences. We also repeated the subsonic filter and ACF calculations for values of v_p of 4 and 5 km s^{-1}. Regardless of the filter selection, the ACF lifetime that resulted was within 10% of the original 3 km s^{-1} filter value.

Figure 6 shows how the ACF of the original data changes with spatial resolution. The solid curve (a) is the original data ACF, and the dashed curve (c) the ACF calculated from data degraded in resolution to 1" by smearing the original frames. Smearing was performed by calculating the Fourier transform of each image in a sequence, filtering in the spatial frequency domain with the appropriate circular aperture diffraction pattern, and then performing the inverse Fourier transform. The insignificant difference caused by loss in resolution probably explains the consistency of ACF results obtained by different observers at many observing sites (see Fig. 2). Because neither the p- nor the f-modes have significant power on the scale of an arcsecond, blurring the data should have little effect if the ACFs are dominated by solar oscillations.

On the other hand, granulation does have significant power on the scale of an arcsecond, so that blurring subsonic data should have a significant effect. Figure 6d also shows ACFs calculated from blurred subsonic filtered data. Here the lifetime of the degraded data (d; *dashed curve*) is doubled compared with the unblurred subsonic data (b; *dotted curve*). Taken together, Figures 1–6 demonstrate that the solar oscillations make a dominant contribution to the temporal ACF

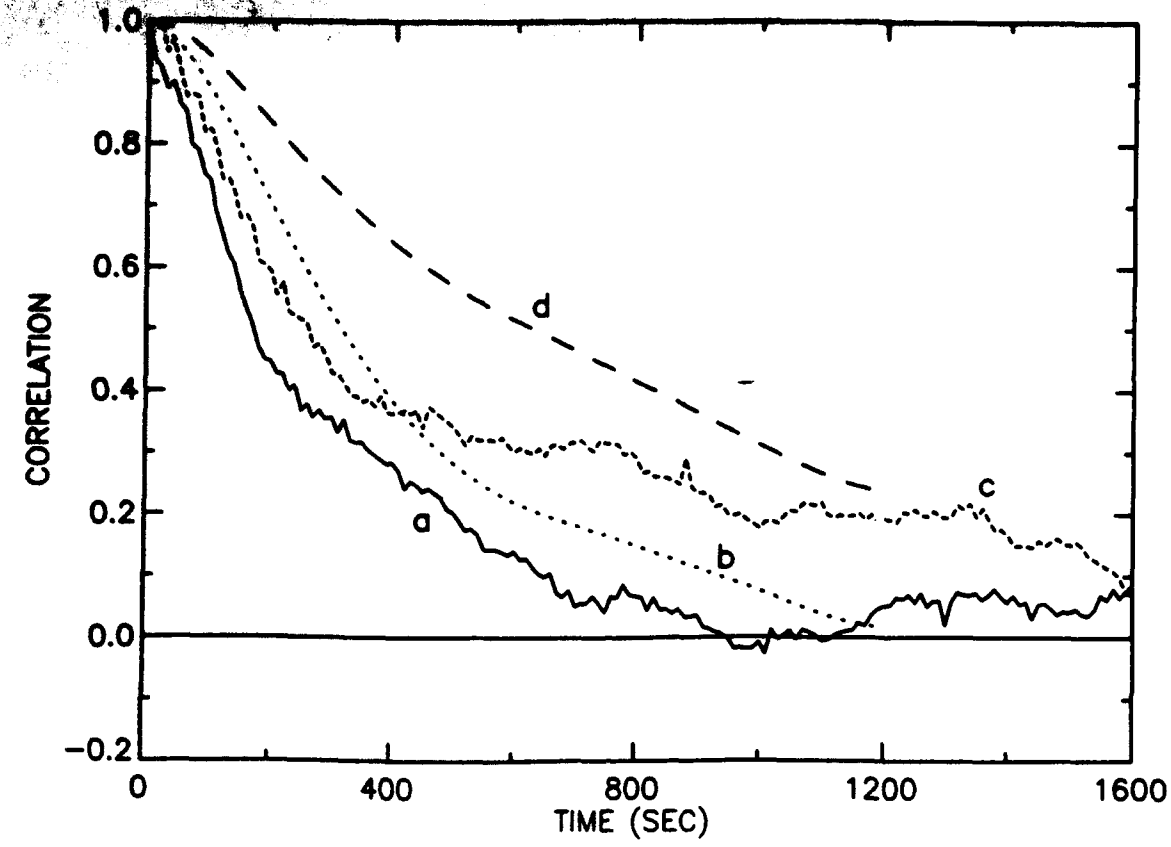

FIG. 5.—Autocorrelation functions (*a*) for quiet Sun original data (Fig. 1*a*), (*b*) for the same data Fourier filtered to remove the effects of solar oscillations, (*c*) for magnetic region original data (Fig. 1*b*), and (*d*) for the same data after Fourier filtering.

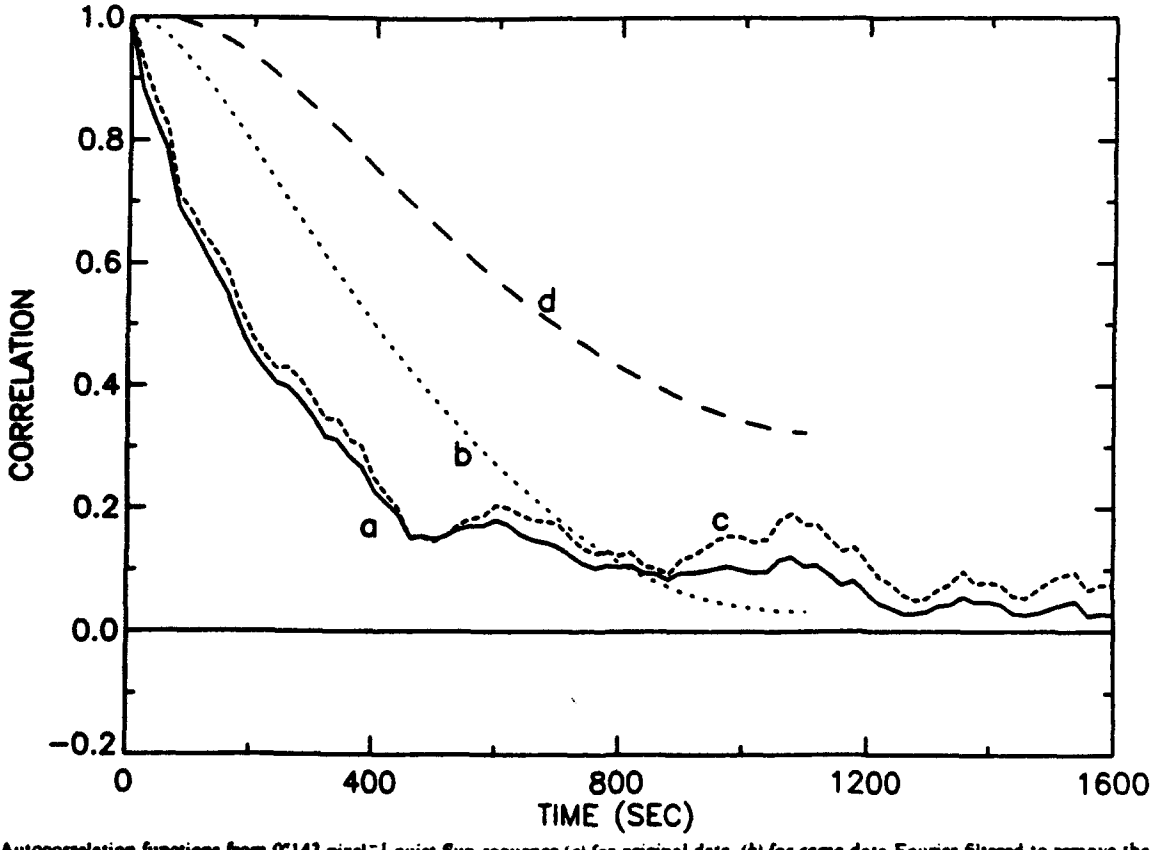

FIG. 6.—Autocorrelation functions from 0".143 pixel^{-1} quiet Sun sequence (*a*) for original data, (*b*) for same data Fourier filtered to remove the effects of solar oscillations, (*c*) for same data as in (*a*) except smeared to 1" resolution, and (*d*) for same data as in (*b*) except smeared to 1" resolution.

and that the characteristics of the granules become apparent only when the oscillations are removed. It also suggests that the differences between quiet and magnetic Sun may be masked by the oscillations present in unfiltered data.

There have long been arguments for the idea that granulation is different in magnetic regions. This was evidenced by a reduction in contrast in magnetic regions—"abnormal granulation" (Dunn and Zirker 1973), increases in granule number density in magnetic regions (Macris 1951), and differences in the shape of the line bisector in photospheric lines in magnetic as compared with quiet regions (Bonet *et al.* 1984). However, because of the variations of granule properties reported by various observers, this evidence has not been convincing. There is also evidence that the mean bisector shape varies with solar cycle (Livingston 1984), and that perhaps the granule density changes with solar cycle (Macris and Rosch 1983).

To observe the effect of magnetic fields on the granulation pattern ACF, 12 boxes were selected inside the 70 G contour of the magnetograms (see Fig. 1, *bottom*) but well outside of pores. The magnetic flux contained within these 12 regions varied from 3×10^{19} to 8×10^{19} Mx. Shown in Figure 7 are the ACFs formed from original (*solid curves*) and subsonic filtered (*dashed curves*) data for four of these boxes. Figure 5 shows a comparison of the summed (all 12 regions) ACFs from original (*c*) and subsonic filtered (*d*) data in the magnetic areas. The lifetime in the magnetic region is more than a factor of 2 greater in subsonic than in original data—890 versus 420 s. Bahng and Schwarzschild (1962) also compared the ACFs in quiet and magnetic areas, but they saw no difference.

Figure 5 summarizes the effects of oscillations and magnetic fields on the temporal ACF. The original data (*a*) in quiet Sun and (*c*) in magnetic regions differ somewhat, while the subsonic filtered data shows substantial difference between (*b*) the quiet Sun and (*d*) magnetic areas. The results are independent of the details of the Fourier filter used. We also repeated these calculations on a second digitized region surrounding the pores. This region was 34" × 34" in size, and therefore had the same pixel size as the quiet Sun region above. These results were in excellent agreement with those shown in Figure 5.

IV. INTENSITY FLUCTUATIONS

The mean intensity of granules in the SOUP passband increases in magnetic field areas, while both oscillations and granule scale intensity fluctuations in time are reduced. The mean intensity and the rms intensity fluctuation over the 28 minute observing interval have been computed in the pore and quiet Sun sequences, for both original and subsonic filtered data. Comparison of the original and subsonic filtered mean intensity images shows that they are virtually identical, because the oscillations present in the original image sequence average out during the 28 minute observing period. The mean intensity image for the pore region clearly shows areas where the granules are brighter, and comparison with a simultaneous BBSO magnetogram reveals that these areas have magnetic fields present.

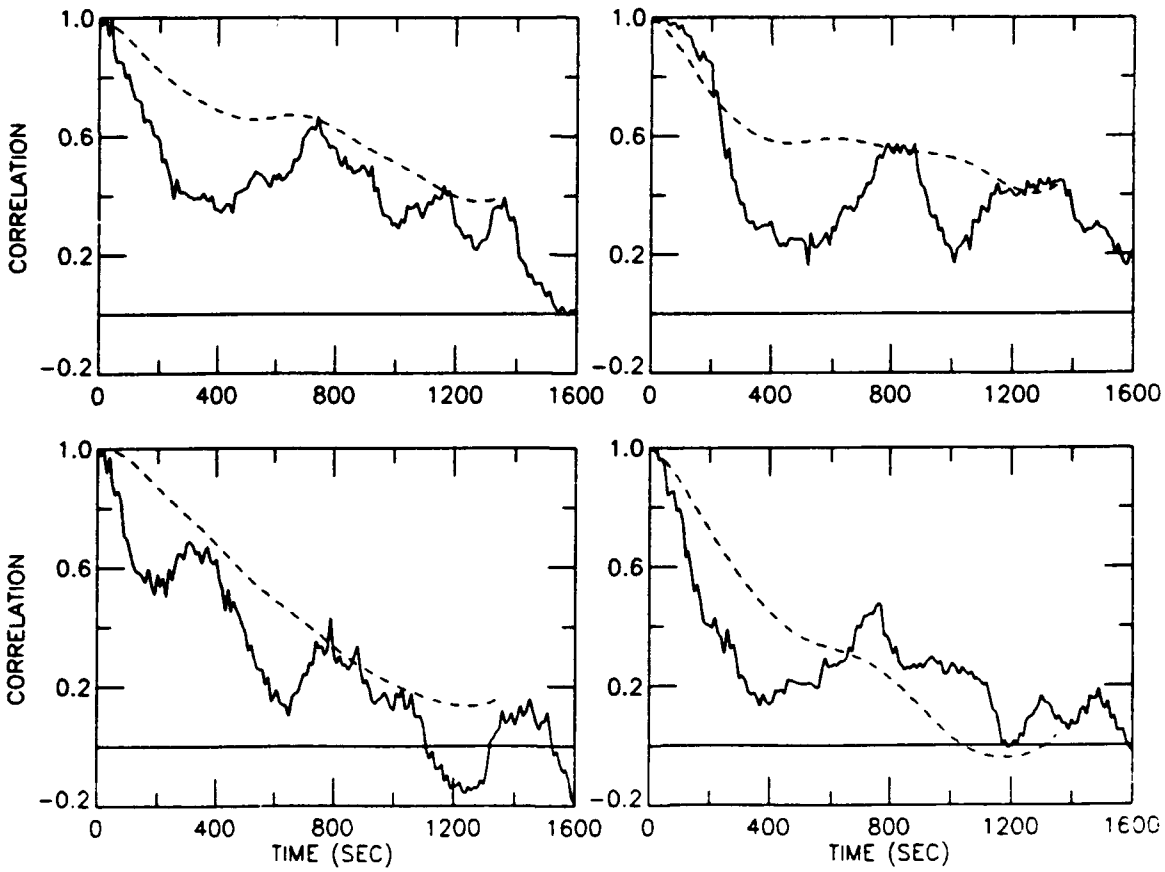

FIG. 7.—Autocorrelation functions in four 6" × 6" boxes of magnetic regions from original (*solid curves*) and Fourier filtered (*dashed curves*) to remove the effects of solar oscillations.

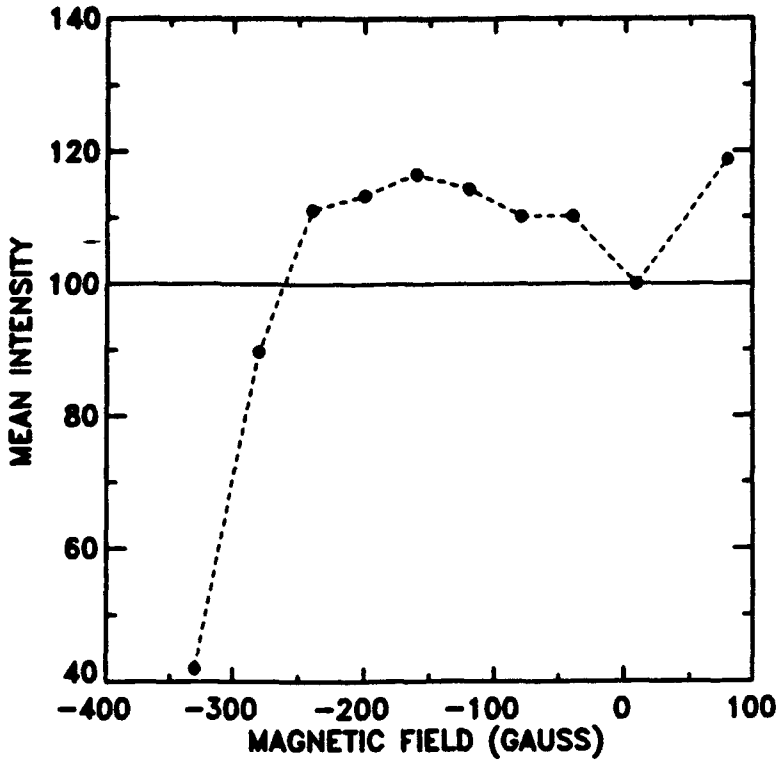

FIG. 8.—Plot of the mean value of intensity in the photosphere as a function of magnetic field strength. The intensities are from an average over 83 images of the pore region spanning 28 minutes. The magnetic field strength is from a registered BBSO magnetogram.

Figure 8 quantifies this result by showing the mean intensity as a function of magnetic field strength. Each data point in Figure 8 is calculated by fitting a Gaussian to the intensity distribution in each magnetic bin, the smallest of which contains at least 1500 image pixels. The size of the error of the mean is smaller than the size of the dots in most cases. The mean intensity at zero field has been normalized to 100. Significantly, as soon as the magnetic field strength is greater than the noise, the mean intensity of granules increases significantly, and remains higher until the field is strong enough for pores to form. The formation of pores is indicated by the sharp drop in mean intensity at −275 G.

Comparison of the rms intensity fluctuations from the original and subsonic filtered image sequences shows that the intensity fluctuations are considerably reduced in the subsonic filtered images. Figure 9 shows the mean normalized rms intensity fluctuation as a function of magnetic field strength for original data (*solid curve*) and subsonic filtered data (*dashed curve*). Also shown in the figure are the values of the rms fluctuations in both sets of quiet Sun data (*diamonds*). In all the movies the rms intensity fluctuation peaks at zero magnetic field, and then declines with increasing field strength until pores form. Note that the point at which Figure 9 shows an upturn is the same magnetic field value where Figure 8 shows a downturn. Pores have significant intensity fluctuations because any change in a pore's size or shape will cause an intensity fluctuation due to the contrast between the pore itself and the surrounding bright granules. These variations within the pore region are consistent with our subjective impression of the "vigor" of the granulation in the movies.

The BBSO magnetogram used in the construction of Figures 8 and 9 has a resolution somewhat worse than 2". This limits the accuracy of its registration to the SOUP images, and our knowledge of the spatial distribution and strength of the magnetic flux. The existence of the relationships shown in Figures 8 and 9 therefore suggests that the presence of a magnetic flux tube affects an area of granulation considerably larger than the diameter of the flux tube.

The diamonds in Figure 9 indicate the value of the rms fluctuations for quiet Sun. The average fluctuation for quiet Sun (subsonic filtered) is about 10% higher than the corresponding value from the zero field regions in plage regions surrounding the pores. Therefore, even the granulation in zero field regions in plage differs from that for field-free quiet Sun. Magnetic effects are not limited to filigree in intergranular lanes.

V. HORIZONTAL FLOWS VIA LOCAL CORRELATION TRACKING

It is apparent from the movies that granules both move randomly and are advected by meso- and supergranulation scale flows. We have measured the horizontal flow velocities by a technique we call local correlation tracking (November *et al.* 1987). Briefly, a coarse rectangular grid of points is chosen covering the image field of view. A spatial cross-correlation between two images (typically 60 s apart in time) is computed in the neighborhood of each grid point. The position of maximum cross-correlation yields a local displacement vector for each grid point. We interpret these displacements as horizontal velocities. The neighborhood of each grid point used for the comparison is defined by a Gaussian apodizing function, and the full width at half-maximum (FWHM) of this Gaussian represents the spatial resolution of the velocity measurement.

We have produced movies of the flow field in this manner by applying local correlation tracking to a time series of image

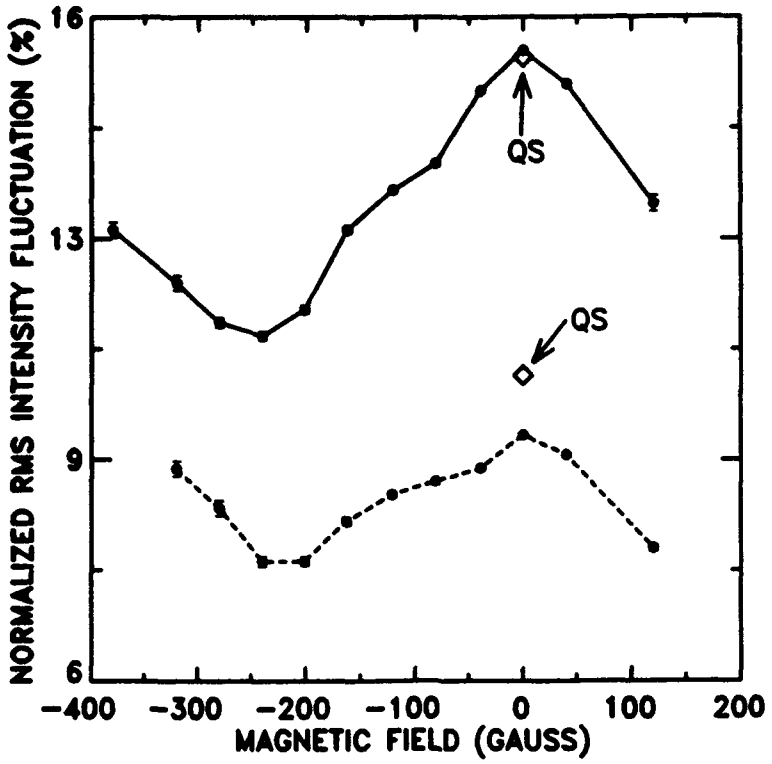

FIG. 9.—Plot of the mean value of the rms intensity fluctuation in the photosphere as a function of magnetic field strength, for original data (*solid curve*) and for Fourier filtered data (*dashed curve*). As in Fig. 8, the rms intensity fluctuations were calculated from a 28 minute long SOUP image sequence centered on the pores. The two diamonds labeled *QS* indicate the mean rms fluctuation at zero magnetic field for a SOUP quiet Sun region.

pairs. Composite movies have been created by overlaying the flow field on the original and subsonic filtered data. These movies clearly show that granules are advected by the flow field, that magnetic regions have smaller steady flows than quiet areas, and that meso- and supergranular scales are visible in the displacement field of the granules (Simon *et al.* 1988). Averaging the velocity over the duration of the movie shows these larger scales clearly, by suppressing flows of individual granules and effects of 5 minute oscillations. Figures 10 and 11 (Plates 11–12) show the average velocity field overlaid on (*a*) an image and (*b*) the divergence of the average velocity field for the quiet Sun and the pore region, respectively. The two-dimensional divergence of the horizontal flow is roughly proportional to the vertical flow (November *et al.* 1987).

The mean flow speed (magnitude of velocity vector) is 370 and 163 m s^{-1} in the quiet Sun and pore region sequences, respectively. Figure 12 shows the histogram of the speeds in the quiet Sun (*left*) and the pore region (*right*). Figure 13 shows a scatter diagram of the flow speed versus magnetic field strength in the pore region. The velocities for Figures 10–13 were calculated using a Gaussian with FWHM of 4″ and a grid spacing of 2″.5. This mask size was chosen to suppress the local expansion and collapse of individual granules but still show meso- and supergranule scale flows. The magnetic field strength is the average from an 8 × 8 pixel area centered at the location where each horizontal velocity vector was calculated. Also marked on Figure 13 is the mean flow speed (*solid*) as a function of magnetic field and the average speed in quiet Sun (*heavy dot*). The mean speed is strongly dependent upon magnetic field; it varies from 275 km s^{-1} at zero field to 100 m s^{-1} for field strengths greater than 175 G. Significantly, the quiet Sun average flow speed is 35% greater than the flow speed in zero field areas near the pores. This implies that magnetic field can affect surface flows for a considerable distance outside the flux tubes themselves. Figures 12 and 13 show clearly that there is a difference between quasi-steady flows in quiet and magnetic regions and that, like the intensity fluctuations, these flows are also different in granulation in zero or low field areas in plage than for field-free quiet Sun.

Besides demonstrating the existence of quasi-steady flow fields, local correlation tracking can also produce estimates of the instantaneous velocities of the granules. The horizontal velocity vector at a single grid point shows fluctuations with time due to granulation, oscillations, waves, and random noise (due primarily to film grain). To separate the noise from the solar signals, we have calculated the Fourier power spectrum of the x and y-components of the velocity in all the points in the image. From the average power spectrum, the white noise level, due primarily to film grain, is easily identified; the rms fluctuating solar velocity and the rms noise can then be calculated. We have measured the velocities using a set of Gaussian masks of FWHM of 4″, 2″, 1″.5 and 1″. The smaller masks show more of the random motions and the rates of expansion and collapse of individual granules, in addition to large-scale flows and oscillations. Unfortunately, the rms noise increases as the width of the mask decreases, so that it is not possible to measure rms velocities at the resolution limit of the images. Shown in Figure 14 are plots of rms speed as a function of Gaussian FWHM for quiet Sun, nonmagnetic areas of the pore region (magnetogram < 40 G), and medium and strong magnetic areas of the pore region (100–400 G and >400 G, respectively).

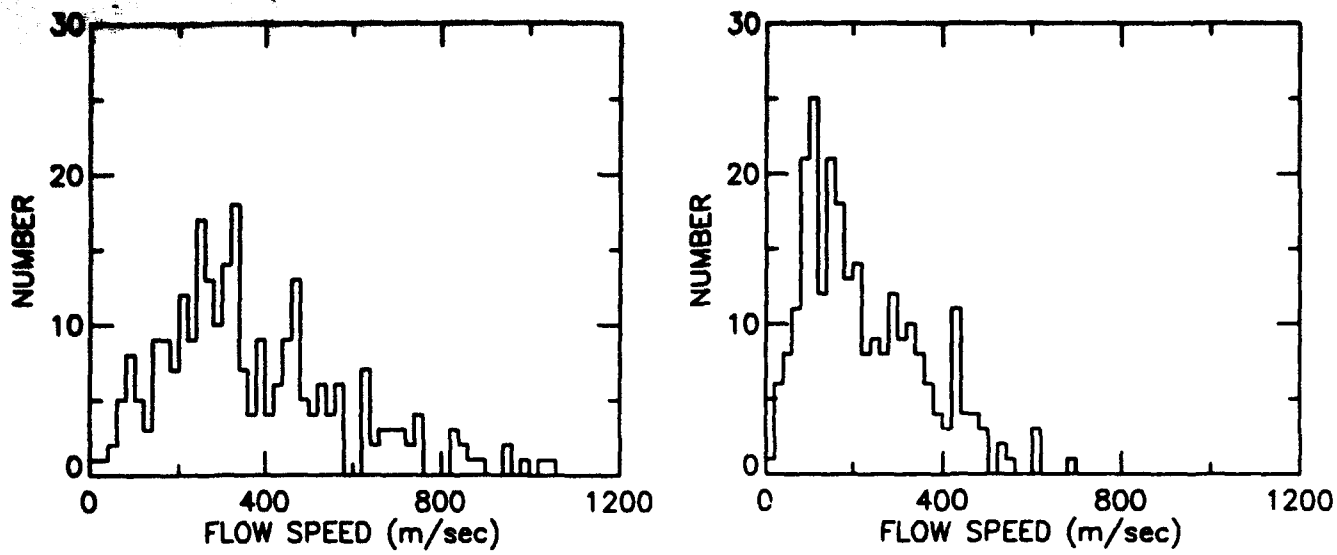

FIG. 12.—Histograms showing the distribution of measured flow speeds in the quiet Sun region (*left*) and pore region (*right*)

The speeds plotted in Figure 14 represent the fluctuating flow at a single point, as measured in different regions and with different spatial resolutions. the sharp increases at finer resolution must be due to granulation, since most power in the 5 minute oscillations is at larger spatial scales. This is borne out by movies of the flow vectors overlaid on the images, in which exploding granules are especially obvious. In strongly magnetic areas, the velocities are systematically 45% less than quiet Sun values. Thus, magnetic fields strongly suppress the vigor of the granulation on 1″ scales. Nonmagnetic locations within the plage are essentially the same as quiet Sun far from strong fields, which implies that the magnetic fields do not affect the vigor of granular flows more than a few arcseconds beyond the boundaries of the flux tubes themselves.

From Figure 14, the rms speed in quiet Sun is at least 1.4 km s^{-1}. This velocity is quite high compared with previous measurements of the vertical component of photospheric velocities (Beckers 1981). It is possible that the local correlation tracking technique is measuring phase velocities as well as mass motion. However, the convective component of the flow is driven by

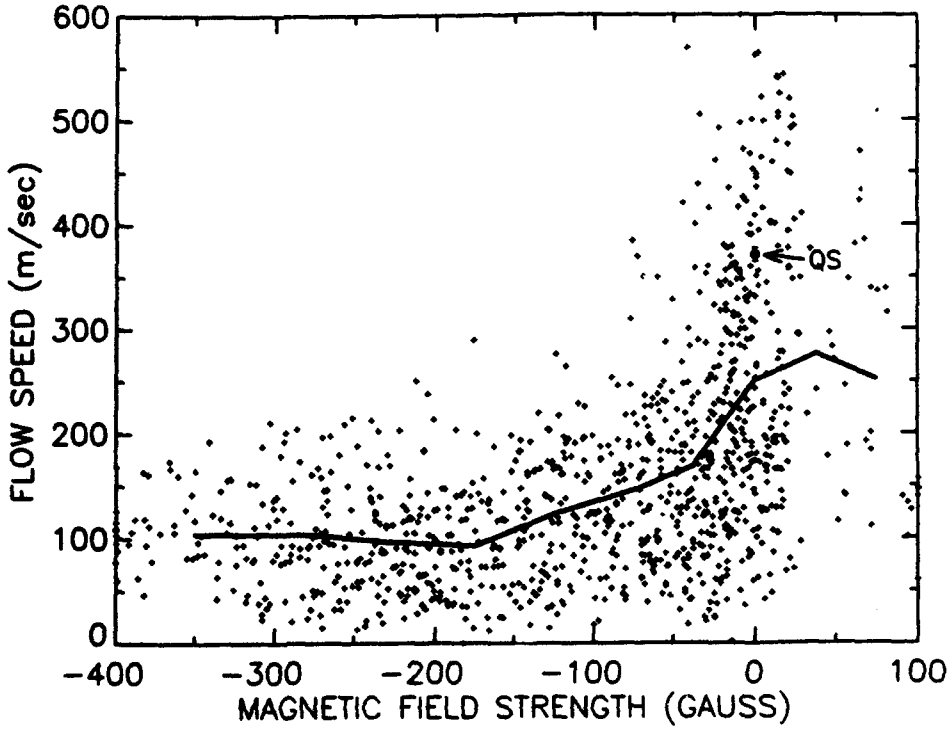

FIG. 13.—Scatter plot showing the flow speed versus local magnetic field strength in the pore region (0″.134 pixel^{-1} sequence). Also indicated is the mean flow speed (*solid line*) as a function of field strength and the mean value from the quiet Sun region (dot labeled *QS* at 0 G).

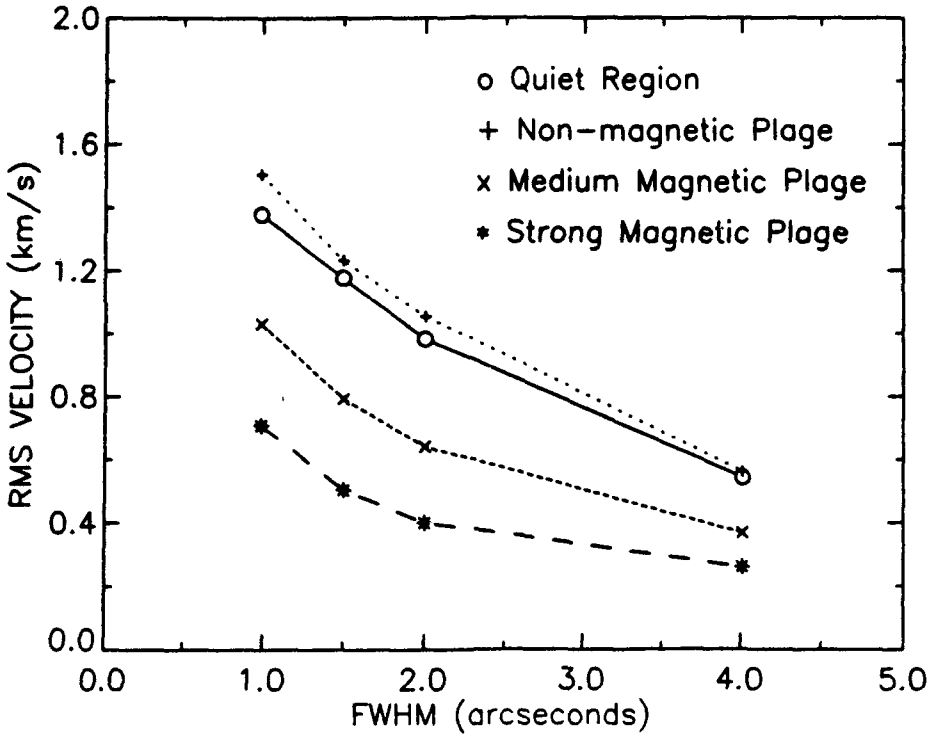

FIG. 14.—Plot showing rms velocity vs FWHM of the Gaussian used in the local correlation technique. Data from different types of regions are designated by open circles (quiet Sun), plus signs (plage), crosses (medium magnetic plage), and asterisks (high-strength magnetic plage).

thermal buoyancy, and radiative losses should cause the brightness front to lag the gas motion. Numerical simulations by A. Nordlund (1988, private communication) verify that brightness fronts lag flows. Thus, our velocities may even underestimate the true values. Details of the relations of brightness and mass flows will be discussed in a separate paper. Nonetheless, the velocities measured here are the correct velocities for understanding how the temporal ACFs evolve.

The temporal ACFs compare sets of spatially aligned data sets as a function of time and yield information related to feature lifetime. Spatial ACFs compare the same image with different spatial offsets and yield information on the spatial scale of the image. The spatial ACF is defined as

$$\mathrm{ACF}_s(\Delta) = \frac{\langle \delta I(x, y, t)\delta I(x + \Delta, y, t)\rangle}{\langle \delta I^2(x, y, t)\rangle},$$

where Δ is the spatial offset. The spatial ACF can be used to estimate the effect of flows on the ACF lifetimes because the displacements can be considered to be the results of a flow. A velocity v which lasts for a time t will cause a displacement $\Delta = vt$. We define a displacement lifetime, T_d, as the time required for the rms flow v_{rms} to cause the spatial ACF to drop to $1/e$:

$$\mathrm{ACF}_s(v_{rms}/T_d) = 1/e.$$

Figure 15 shows (*a*) the spatial ACF for subsonic filtered quiet Sun and (*b*) the spatial ACF for magnetic regions. From the figure the $1/e$ width is 450 km and 500 km for quiet and magnetic regions, respectively, which is consistent with previous measurements (Wittmann 1979). On average, structures in the quiet and magnetic regions are about the same size in the SOUP images. While we have shown that granules in the magnetic region are different from quiet granules, the spatial ACF is not a good discriminator of that difference. Nevertheless, the eye can see a subtly different texture in the magnetic parts of the pore region in single images.

Either random or locally ordered motions will cause the lifetime measured from the temporal ACF to underestimate the lifetime of the individual features in the granulation field. Using a velocity of 1.4 km s^{-1} for quiet Sun, the displacement lifetime T_d is 320 s, compared with an ACF lifetime of 270 s. In the medium magnetic plage (see Fig. 14), we use 1.0 km s^{-1}, which yields a T_d of 500 s, compared with 420 s from the ACF. Thus, in both cases, the flows are sufficient to cause much of the decay in the temporal ACF. Note that this flow includes not only the displacements of entire granules but also some of the distortions and explosions which are seen by the local correlation tracking with a 1″ FWHM Gaussian. The temporal ACF does not simply reflect the lifetime of isolated intensity features in granulation: motion and distortion of the features have a large effect.

VI. GRANULE TRACKING

Because of random and ordered motion, the temporal ACF yields a poor estimate of the lifetime of individual features in the granulation pattern. The direct method for determining lifetime is to identify and then track individual features in the pattern. The standard approach has been to find a granule on a master frame and then to track it as long as possible on following and preceding images (Mehltretter 1978). The weakness of all human identifications is the biased selection of the tracked elements and the determination of the beginning and end points. This is especially true because the majority of granules are born from an existing fragment (Dialetis and Macris 1984;

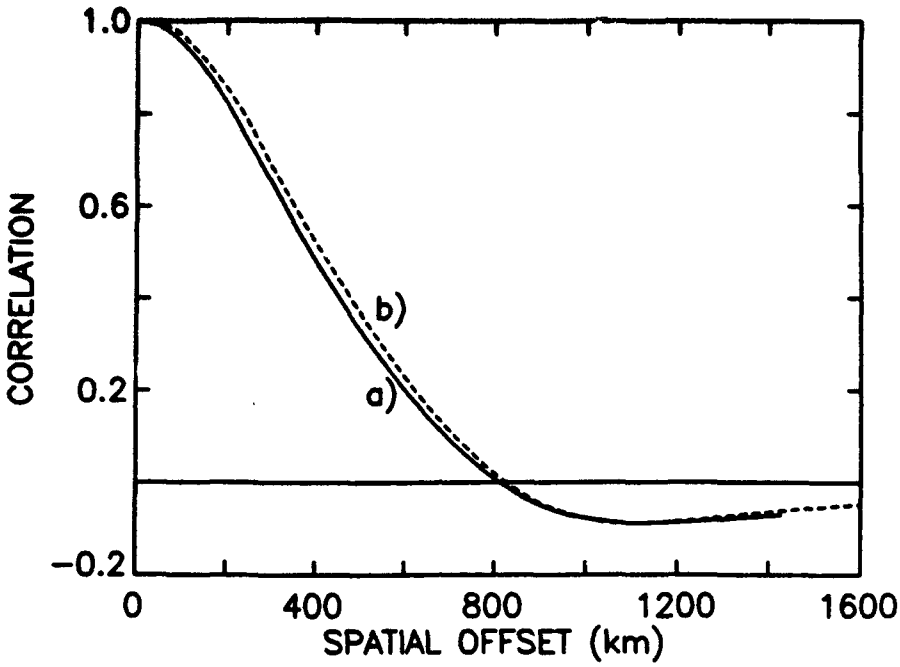

FIG. 15.—Spatial autocorrelation measurements for (*a*) subsonic filtered quiet Sun and (*b*) subsonic filtered magnetic region

Mehltretter 1978). Since our images are free of distortions caused by atmospheric turbulence, we have tried to develop unbiased computer procedures for identifying and then following granules.

The first step toward tracking granules is to identify all of them. We have tried two different algorithms, which we call "center finding" and "lane finding." The first is based on finding locally brightest points and identifying them with granule centers, and the other on finding the intergranular lanes which surround each granule. In other words, center finding finds granule centers directly by identification, and lane finding finds their boundaries and infers a center in the middle of an enclosed area. Both these families of methods suffer from the problem that a "granule" may have an internal structure with multiple bright points or multiple dark lanes during its lifetime.

All center-finding algorithms are based on exploring a local neighborhood and finding the bright points in that area. The simplest of these methods is based on thresholding—defining granules as the connected areas above some intensity threshold. Pure thresholding methods are very sensitive to intensity variations over the frame caused by seeing and solar oscillations. To make them relatively stable, a spatial filter must be applied to the images to remove very high and very low spatial frequencies (Roudier and Muller 1987). We have experimented with thresholding, but we feel that it is too sensitive to low spatial frequency intensity variations, and to the detailed form of the spatial filter used.

Instead, our center-finding algorithm searches for local maxima by comparing the brightness of every point in the image with its neighbors. The test depends upon two parameters, which are the value of the intensity delta by which a center must exceed its neighbors and the size of the neighborhood examined. Shown in Figure 16 (Plate 13) is (*a*) a typical granulation frame and (*b*) the same frame with the centers marked. The intensity delta has been adjusted to give a satisfying result for (*b*). The number of centers found is reasonably insensitive to the size of the local neighborhood examined in a range from 0".4 to 0".9 (3–7 pixel width). The average number of granules identified by this algorithm is 500 in a 1600 arcsec^2 area of quiet Sun, or 31 granules per 100 arcsec^2, about the mean of values found by previous observers (Wittmann 1979). Based on this statistic, the center-finding algorithm is finding most of the larger granules, but not the fine structures within them, and not the smallest features.

The lane-finding algorithm is much more sophisticated. It isolates local bright areas by surrounding them with a boundary lane. The granule location is then defined as the center of gravity of each individual hole in the lane net. Figure 16*c* shows the quiet Sun frame overlaid by the lane net with the granule locations marked. About 1000 granules were found by the lane-finding procedure, or 63 granules per 100 arcsec^2, which is in the range found by Namba and Diemel (1969) and Karpinsky (1980).

A comparison of the center- and lane-finding results is shown in Figure 16*d*, where the granulation mesh is shown filled in in white wherever the center-finding algorithm failed to identify a granule found by the lane-finding algorithm. (The instances where a single granule found by the lane finder was identified as two or more granules by the center finder is very rare). By inspection, we see that the lane finder located small features missed by the center finder, and also subdivided some of the larger granules. The granule density in the white area of Figure 16*d* is 140 per 100 arcsec^2. With the assumption that granules are in a roughly hexagonal close-packed pattern, the granule center-to-center distance is 1".9, 1".35, and 0".9 for densities of 31, 63, and 140 granules per 100 arcsec^2. Again these numbers bracket the range found by previous observers (Wittmann 1979).

The results of the lane-finding algorithm can be used to measure the area of each granule, and this allows us to generate a number of statistical properties similar to those generated

by Roudier and Muller (1987). Our areas are that of the mesh that isolates a granule. We will define the "granule" size to be a circle that has two-thirds the area of the mesh. We do this so that the area of the granules and that of the intergranular lanes are approximately equal. The exact ratio of granule to lane area has little effect on the character of the statistical relations.

Figure 17 shows a histogram of granule number versus size, for both lane-found (*solid line*) and center-found (*dashed line*) granules. The number of lane-found granules increases monotonically toward smaller size until a cutoff is reached due to the resolution limit of the SOUP telescope. This means that SOUP cannot resolve all of the granules present, a fact confirmed by higher resolution ground-based observations that reveal structures smaller than the SOUP resolution limit. Figure 18 is a histogram of fractional area occupied by granules of a given size versus size. Both curves show a broad peak between 0".8 and 1".5, in agreement with Roudier and Muller (1987). Figure 19 contains the distribution function of center-to-center distances. The peak of this distribution is determined mainly by the observed number of granules per unit area and is nearly independent of the identification algorithm used. The area distribution (Fig. 18) is a reasonable representation of the length scale of granulation. Even if there may be a large number of unresolved small granules, their contribution to the total area is small, so that it is fair to say that there is a characteristic granule size in the vicinity of 1".2–1".4.

However, we see no evidence for the abrupt change in granule properties at 1".3 reported by Roudier and Muller (1987). Since the change occurs in the largest granules, the resolution difference should not be critical. From inspection of their filtered images, we believe that the change is due to the effect of their high-pass filter and threshold processing on the largest granules. Large, relatively smooth intensity features develop long, sinuous perimeters which are artifacts of the identification algorithm.

Given a set of images with the granule centers marked, it would seem straightforward to identify the center of the same granule on sequential movie frames. In fact, because of the tendency for granules to develop multiple centers or multiple lanes, the objective identification of the beginning and end of a granule is difficult both conceptually and computationally. For our algorithm, identification occurs if granule centers on successive images are separated by less than a tolerance Δr. By examining the entire movie starting on the first frame in which identification is possible and then continuing until identification is no longer possible, we obtain sets of x, y, and t coordinates of associated granule centers. Each association forms a trajectory in three-dimensional spacetime, which we call a "string," from which we can measure the velocity and lifetime. Because the string algorithm looks at each frame in succession, it will not, in general, properly connect a granule that fragments and then re-forms.

Figure 20 contains six plots of the number of granules with lifetime t as a function of t. It illustrates both center-found and lane-found granules in both original and subsonic filtered data, for Δr of 0".5 and 1". All of the plots are well fitted by an exponential decay,

$$N(t) = N_0 \, e^{-t/T},$$

where $N(t)$ is the number of granule strings of lifetime t, and T is the mean granule lifetime.

The granules found by the center-finding algorithm yield a mean lifetime of about 5 minutes, and the granules found by the lane-finding algorithm have a somewhat shorter lifetime. These values are similar to those of Kawaguchi (1980), who followed granules from fragmentation to fragmentation. Increasing the value of Δr does not increase the apparent lifetime but rather causes it to decrease. This is because increasing the value of Δr causes the string algorithm to match granules that are close together spatially but are otherwise unrelated.

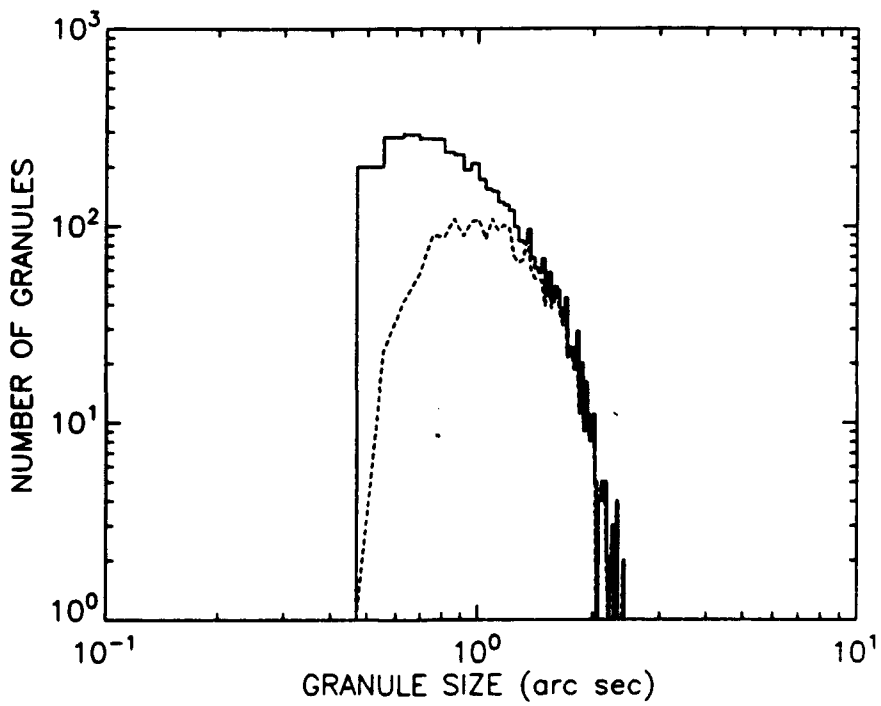

FIG. 17.—Histogram showing the size distributions of granules found by lane finding (*solid lines*), and by center finding (*dashed lines*)

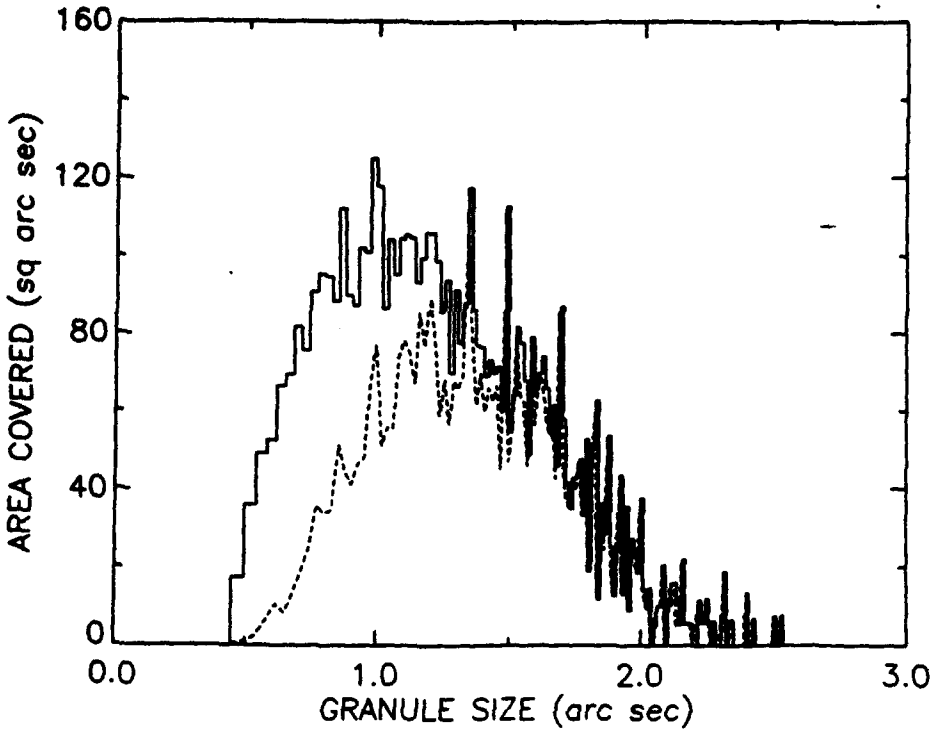

FIG. 18.—Histogram showing the area covered by granules as a function of their size for granules identified by lane finding (*solid line*) and by center finding (*dashed line*).

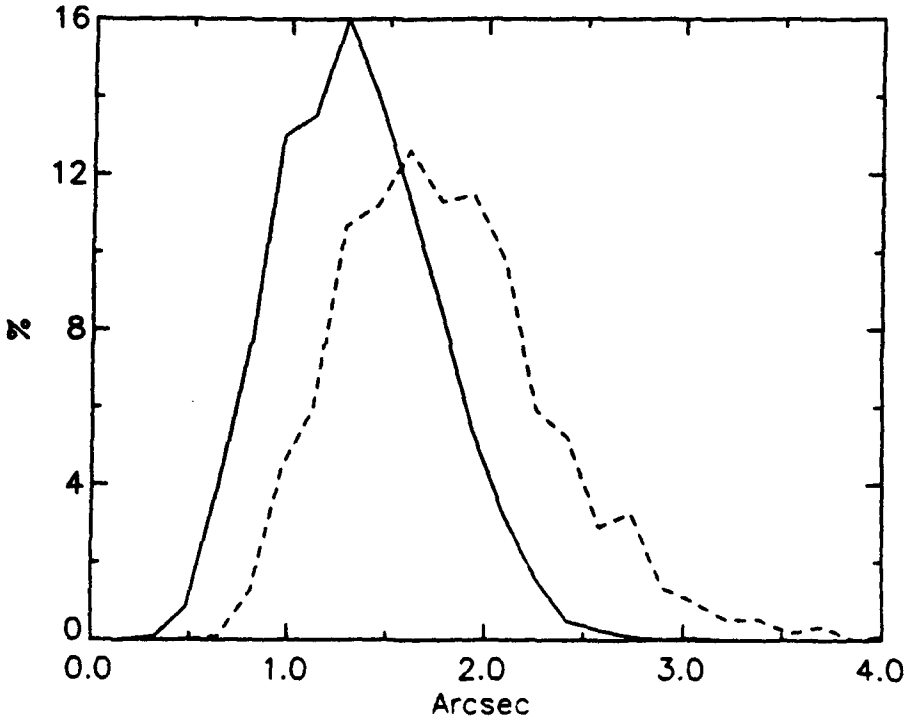

FIG. 19.—Observed distribution in granule center-to-center distance using lane-found granules (*solid line*) and center-found granules (*dashed line*)

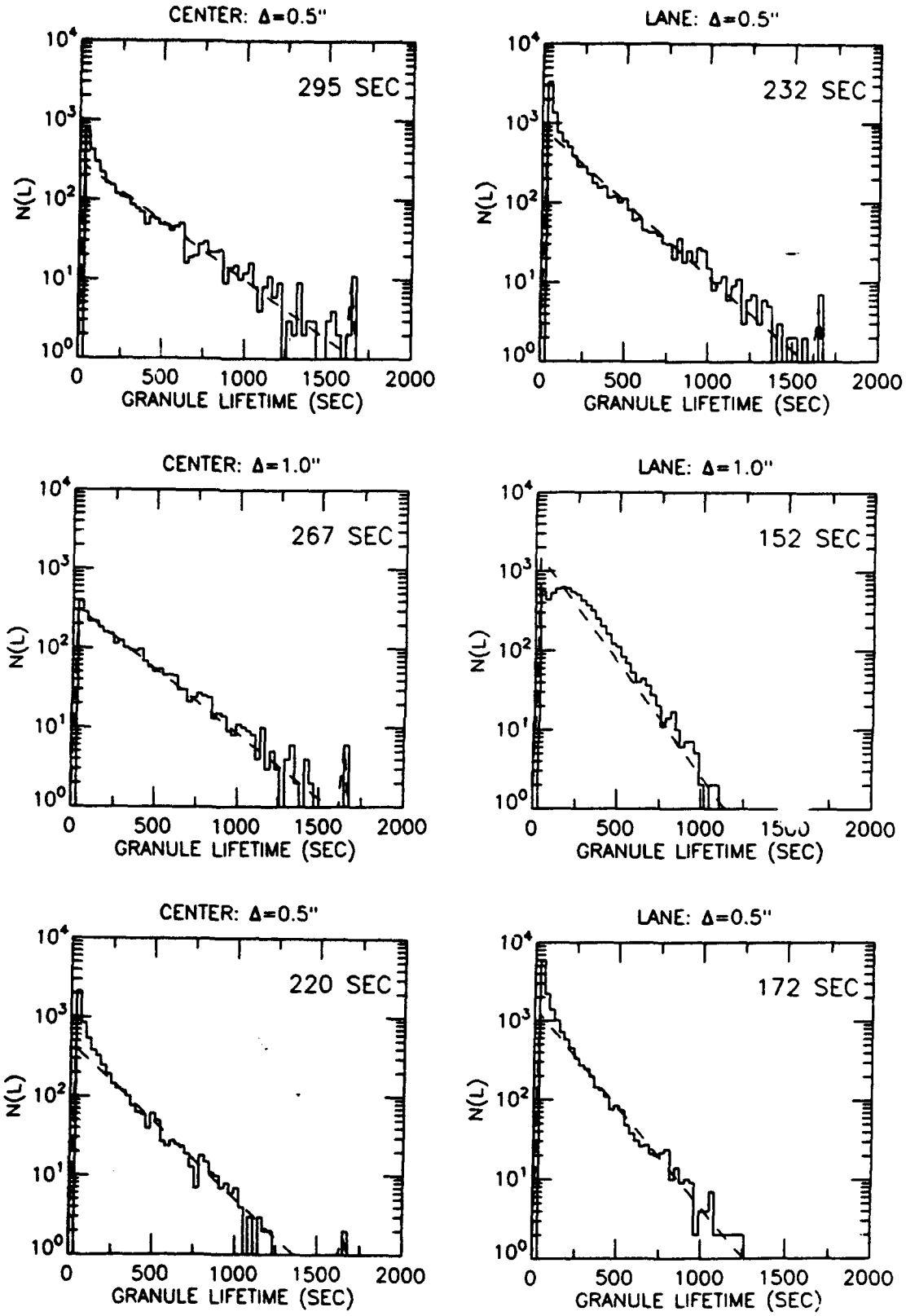

FIG. 20.—Histograms of granule lifetimes for Fourier-filtered quiet Sun data using (*top left*) center finding with $\Delta r = 0''.5$, (*top right*) lane finding with $\Delta r = 0''.5$, (*middle left*) center finding with $\Delta r = 1''.0$, (*middle right*) lane finding with $\Delta r = 1''.0$, (*bottom left*) original data using center finding with $\Delta r = 0''.5$, and (*bottom right*) original data using lane finding with $\Delta r = 0''.5$.

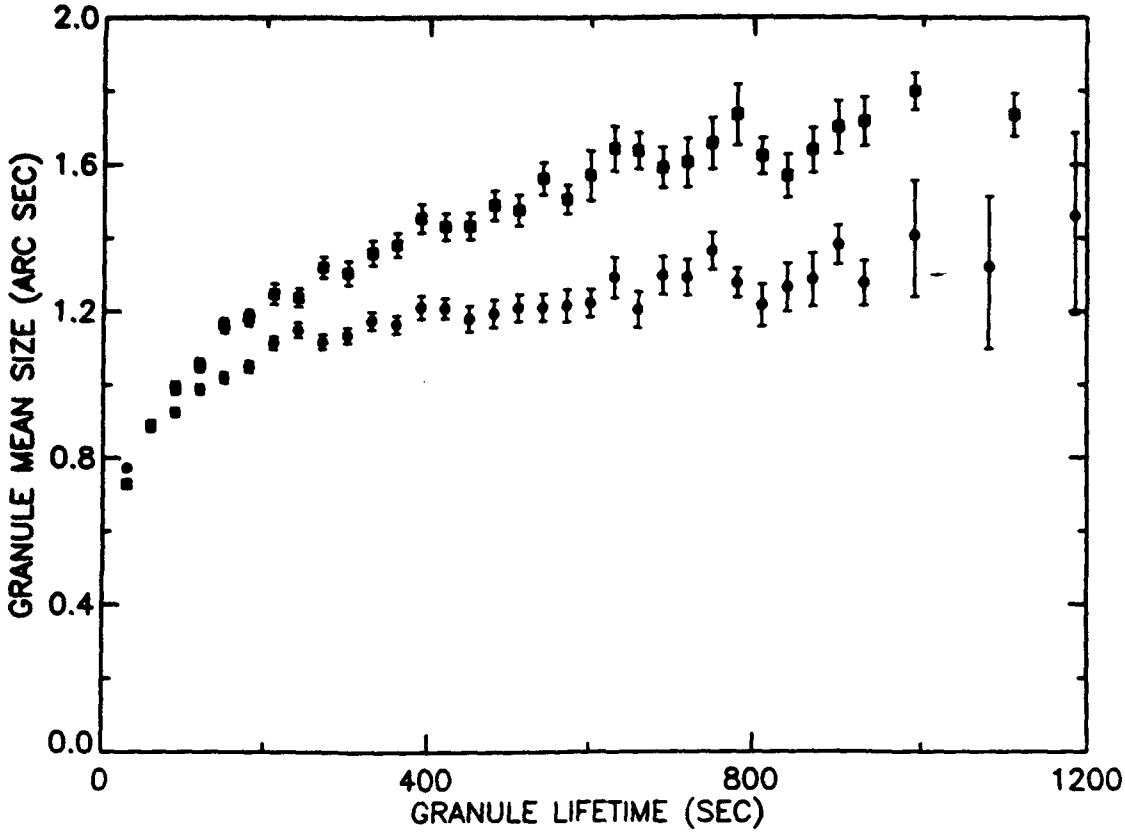

FIG. 21.—Mean size of granules as a function of their measured lifetime. The filled circles refer to the mean of the lifetime-average size of each granule during its lifetime, while the filled squares are the means of the maximum size of the same granules.

For each granule string we have determined the lifetime-average and maximum size. Figure 21 shows a plot of the mean value of both the lifetime-average size (*filled circles*) and maximum size (*filled squares*) of granules as a function of their lifetime. It is the result of averaging over 9500 individual granule strings. The mean of the lifetime-average granule size increases by nearly 60% as the lifetime increases from 30 to 400 s, and then changes little with lifetime after that. For the shortest lifetimes the means of the lifetime-average and maximum granule sizes are nearly the same. The shortest-lived granules have little time to change size, and may be visible on as few as two images. After 300 s, however, there is a nearly constant difference of 25% between the mean value of the lifetime-average size and the mean value of the maximum size. Figure 22 shows the area of the movie covered by features with a lifetime t. In contrast to Figure 18, it shows no tendency to peak at some characteristic time.

We have used the results of our granule string-finding algorithm to study the spatial distribution of granules with different lifetimes. Maps have been produced showing the location within our field of view of all granules with a lifetime within a certain range. These maps have been carefully compared with the horizontal flow field by superposition with maps of the divergence of the flow, such as those shown in Figures 10 and 11. In general, granules appear to be randomly distributed on the surface of the Sun, independent of their lifetimes. In particular, the longest-lived granules show no preference for occurring inside of, or on the boundaries of, mesogranules and supergranules.

The string-finding algorithm does not yield granule lifetimes longer than those measured by either the original or the subsonic temporal ACFs. Lifetime results are potentially very sensitive to the efficiency at which the string-finding algorithm matches granules on successive frames. Given a sequence of images with 10 s spacing and a granulation pattern with infinite lifetime, our algorithm would find a lifetime of 300 s or less if its frame-to-frame efficiency were 97% or less. Measuring the efficiency of the algorithm is nearly impossible, because of the ambiguity between real misses and misses due to granules just being born, just fragmenting, and just dying. To get around the efficiency problem, we have repeated the calculations allowing for breaks of one and two frames in the granule strings, so as to correct for noise in a few frames that might otherwise artificially end a granule's life. String mending did not substantially modify the lifetime results.

We have also attempted to follow granules visually from birth to death on our movies. In almost all cases examined, the granules do begin and end as the string-finding algorithm finds. However, this is not surprising after viewing the movies, which show many exploding granules and granules with complex internal structures. Below we will discuss exploding granules, which may offer some explanation of the apparent lack of success of string finding, and give some insight into the evolutionary processes in the photospheric intensity field.

Since our string-finding algorithm can follow only one of the granule fragments when a granule subdivides, we have tried to learn more about granule lifetimes by first degrading the resolution to 1″ before string finding in an attempt to mitigate

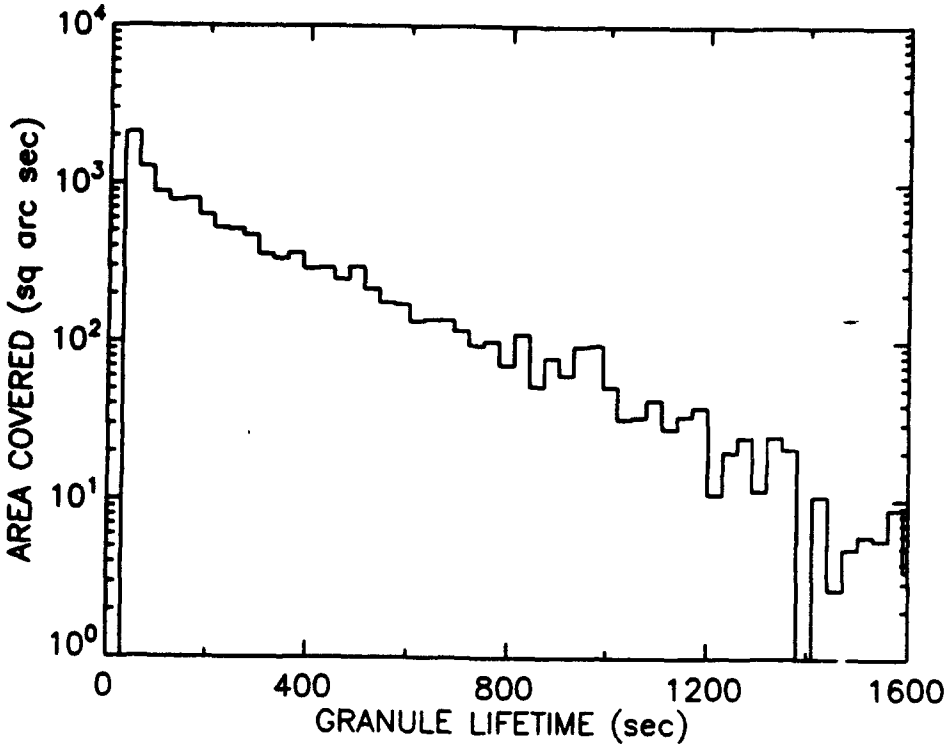

FIG. 22.—Area covered by granules as a function of their measured lifetimes

the effects of fragmentation. Smearing was done by appropriate filtering in the Fourier domain. Note that the smeared images are not equivalent to atmospheric "seeing" because they are still free of distortion. Figure 23 shows a histogram of number of granules with lifetime t as a function of t for the smeared images. Using the lane finder, the density of granules found is 21 per 100 arcsec^2 and the mean lifetime is about 10 minutes. The total number of granule strings found is down by a factor of about 10 when compared with the original data.

Our string-finding algorithm has been very useful for measuring granule velocities, because it produces x and y-coordinates of the center of the granule throughout its lifetime. We have fitted a straight line to each of these sets of coordinates. The slope of this line is the mean horizontal velocity of the granule. Shown in Figure 24 is the mean velocity, and the standard deviation of the mean, as a function of granule lifetime. There is an indication that short-lived granules move at a mean velocity of about 1.2 km s^{-1}. For the longer-lived gran-

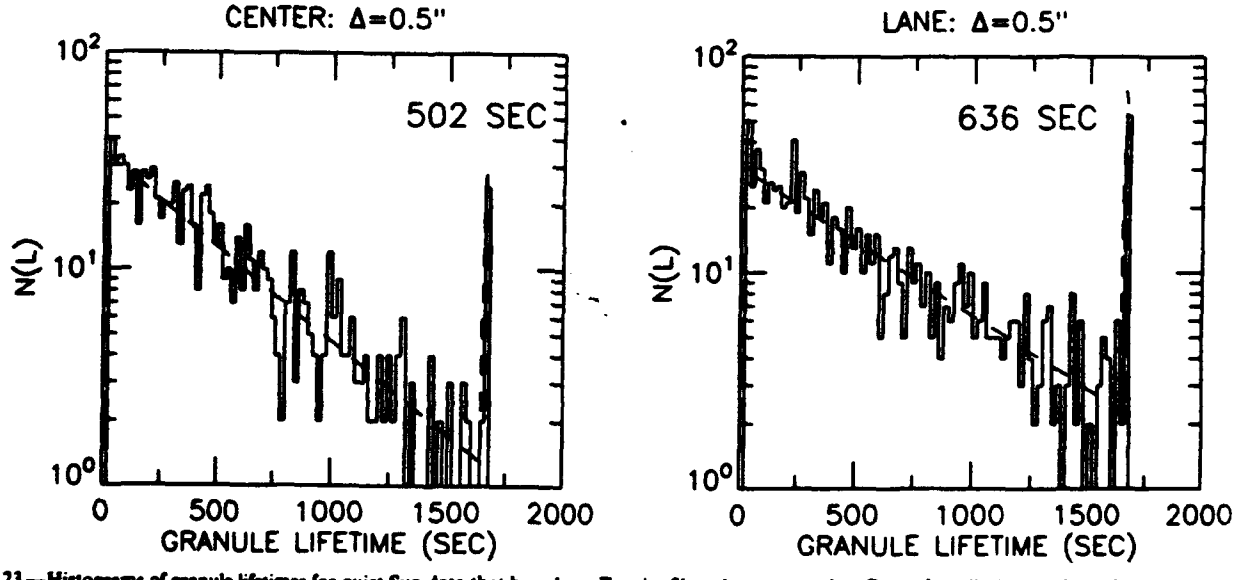

FIG. 23.—Histograms of granule lifetimes for quiet Sun data that have been Fourier filtered to remove the effects of oscillations and also have been smeared to a resolution of 1", using center finding with $\Delta r = 0''.5$ and (*left*) using lane finding with $\Delta r = 0''.5$ (*right*).

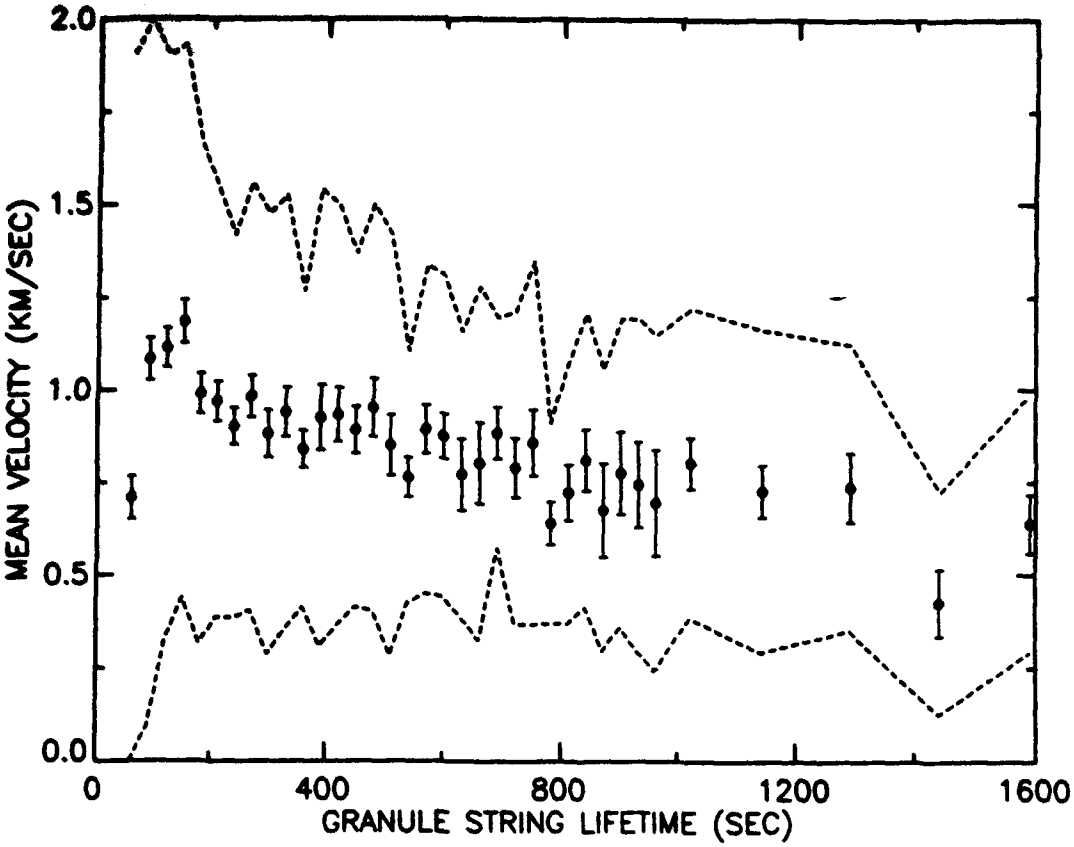

FIG. 24.—Mean random velocities of granules as a function of their lifetime, derived from tracking each granule center during its lifetime. The dashed lines are $\pm 1\,\sigma$ in the distribution of observed velocities.

ules the mean velocity is 750 to 850 m s^{-1}. This is consistent with the speeds measured by local correlation tracking with mask sizes of about 1".5, which includes granule motion but excludes granule expansion and contraction.

VII. EXPLODING GRANULES

Granules that expand radially and develop a dark central region were discovered by Roach and his coworkers (Carlier *et al.* 1968) and given the name "exploding granules." A prototypical example is shown in Figure 25 (Plate 14). Usually the expanding ring is not a complete symmetrical structure as seen in the figure, but rather an ensemble of local brightenings which are all travelling outward from a center. They are rather rare in earlier granulation data (Mehltretter 1978; Namba and van Rijsbergen 1977), but in SOUP data they are common. Kitai and Kawaguchi (1979) have noted the presence of a dark central spot in a large fraction of granules, but not all of these have a radial expansion phase. Referring to the occurrence of exploding granules, Beckers and Canfield (1975) wrote, "We would not consider it at all unlikely that all granules would show a similar behavior if the quality of the observation were good enough." Recently Steffen, Ludwig, and Kruss (1988) calculated that the "exploding" configuration is the steady state form of granulation.

We have used spatial-temporal maps, "time-slice" images, to measure and quantify the behavior of individual exploding granules. These images show intensity as a function of time along a line on the Sun. In a time slice an ordinary granule appears as a bright tube of some length and inclination to the ordinate. An exploding granule appears as a Y shape, and, when the chosen line crosses the spatial center of the exploder, the Y has its maximum opening angle. The tilt of the arms of the Y is the radial expansion velocity of the exploder. Measurements of the tilts show expansion velocities in the range 1–2 km s^{-1}, which is consistent with values measured by Musman (1972) and Namba (1986). Figure 26 (Plate 15) shows time slices through the center of five exploding granules.

We have studied intensively the central 32" × 32" of the 40" × 40" quiet Sun region, and have found 41 clear examples of exploders in the 1360 s movie. The central region was used to avoid misidentifying exploding granules occurring at the edges of the region. The average diameter of the cells at maximum expansion is about 4".2. Because it is hard to recognize an event unless the initial center or the final ring can be seen, a total of about 360 s at the beginning and end of the movie are lost for detection. This suggests that at least 4.0 exploding granules are born in a 10" × 10" area during the movie, if they were distributed uniformly. This is a lower limit, since, owing to the relatively high density of exploders, some events will not be recognized because of overlap and interference.

Allen and Musman (1973) and Oda (1984) have shown that exploding granules are not statistically associated with the supergranulation network. Oda (1984) found some evidence that growing granules may be associated with mesogranulation. Figure 27 (Plate 16) shows the map of the divergence of the horizontal flow pattern overlaid by the location of exploding granules. Only one exploding granule is well inside a

region of negative divergence. The strong tendency of exploders to occur in mesogranules at a high rate is probably the reason other observers have noted that exploding granules repeat and spawn new exploders (Carlier *et al.* 1968; Kawaguchi 1980). Of course, it also means that all granules do not explode.

Since regions of positive and negative divergence have nearly equal areas, about eight exploding granules per 10″ × 10″ area per 1000 s are born in cell-center regions during the duration of the movie. The mean area of maximum expansion of an exploding granule is about 14 arcsec^2, hence 150 arcsec^2 of the average 10″ × 10″ area are impacted by exploders during the 1360 s of the movie. This means that in every 900 s or less such regions are swept by the expansion fronts of exploding granules. It is hard to avoid the conclusion that virtually all the granules that appear in the centers of mesogranulation cells either explode, are pushed aside, or are terminated by an exploding granule in their vicinity. It also means that granules born in the region of negative divergence are constrained from exploding. In both cases, explosions are a major factor in determining the lifetime of granules in quiet Sun. These conclusions are verified by observations of the SOUP and La Palma (Brandt *et al.* 1988) movies.

VIII. DISCUSSION

We have attempted in this paper to use computer algorithms and statistical techniques to identify, measure, and quantify properties of solar granulation. Such a plan is complicated by the richness of the phenomena on the solar surface. The intensity pattern of the solar photosphere is due to granulation (convective overshoot and turbulent flows), oscillations (*p*- and *f*-modes), local internal gravity waves, and magnetic fields. From a single photograph it is impossible to separate these phenomena. With the SOUP time sequences of images most of the effects of global oscillations, and some of the effects of the waves, can be separated from the intensity pattern. Simultaneous magnetograms have allowed us to isolate some of the effects of magnetic fields as well. In spite of the difficulties in some areas the initial plan has been successful, and we have found the following.

1. The temporal ACF of the photosphere is dominated by the presence of solar oscillations rather than by the evolution of granulation. If sufficiently small areas of the photosphere are studied, the ACF oscillates with periods of 3–6 minutes. When the solar oscillations are removed by Fourier filtering, the temporal ACF of the photosphere shows an approximately exponential decay. The decay lifetime in magnetic field areas is about twice as long as in quiet Sun areas, which indicates significant differences between the evolution of granulation in quiet and magnetic Sun.

2. The quasi-steady component of the horizontal velocities of granules averages 370 m s^{-1} (with 4″ mask size) in quiet Sun. The patterns in this flow are on the scale of meso- and supergranules. Magnetic fields strongly inhibit the average horizontal flow speeds of granules, to 275 m s^{-1} for weak fields and to 100 m s^{-1} for strong fields. In plage regions of nearly zero magnetic field the steady flows are down by 10% from field-free quiet Sun.

3. Measurements of the rms fluctuating horizontal velocities are strongly dependent on the type of solar region and the size of the aperture used for correlation tracking. In quiet Sun these velocities go from about 0.45 to 1.4 km s^{-1} and in strong magnetic regions the increase is from 0.3 to 0.75 km s^{-1} as the measurement aperture decreases from 4″ to 1″. The velocities measured by the smallest apertures are on the order of velocities required for models of solar line widths. The rms velocities are lower in the magnetic field areas by about 45%.

4. The horizontal motions of granules alone are sufficient to explain much of the decay of the temporal ACF. Thus temporal ACFs do not measure the lifetimes of granules; but rather, they measure the evolution of the patterns in granulation.

5. On average, granules are brighter in magnetic field areas than in quiet Sun, and the magnitude of the intensity increase is nearly independent of field strength until pores form. Temporal intensity fluctuations are a maximum for quiet Sun and decrease as magnetic flux in the local neighborhood increases. The fluctuations decrease monotonically with increasing field strength until pores form. The effects of magnetic fields on granulation extend well beyond (perhaps 2″–4″ or more) the boundaries of the individual magnetic flux tubes.

6. Attempts to measure parameters such as the mean granule size, the granular density, and the mean intergranular spacing yield results that are algorithm-dependent as well as resolution-dependent.

7. Attempts to measure the lifetimes of all granules on an objective basis yield an average lifetime of about 5 minutes. Degrading the resolution of the SOUP images to 1″ in an attempt to reduce the effects of fragmentation increases the lifetime to about 10 minutes. The granules with the shortest lifetimes are the smallest and have the largest random horizontal velocities. The longest-lived granules appear to be randomly distributed with respect to the mesogranules and supergranules.

8. Exploding granules tend to occur inside of mesogranules—in regions of positive divergence of the horizontal flow. Every 900 s, on average, all of the area within these cells has been affected at least once by the expansion fronts of an exploding granule. This also means that the evolutionary history of granules located within the network between mesogranules is very different from that of granules within the cells.

The mesoscale advective flow may be sufficient to account for the exploders, or a nonuniform energy input associated with the mesogranules may cause the thermal plumes in the centers of these cells to be more vigorous. Modern hydrodynamic calculations may yield insight into the proper role of mesogranulation.

In 1962 Leighton noted that there is an asymmetry between the granules and the intergranular lanes visible on the best-quality photographs. He then argued that granulation consists of convective cells rather than turbulent flows. In 1987 Roudier and Muller determined that the number of granules per unit area increases monotonically with decreasing size, and they argue that this is evidence for a turbulent origin for smaller granules. Our observational results substantially agree with both of these authors.

It is easy to imagine that granulation results from random vertical flows of thermal plumes penetrating upward into the photosphere. When the plumes reach the convectively stable layer, they begin to expand horizontally, become unstable, and break up into a turbulent cascade with a Kolmogorov spectrum. We will resist forming conclusions for now. Rather, we will defer them to further reports on the detailed behavior of granules in regions of convergence and divergence based on ground-based observations at the new Swedish Observatory on La Palma.

When this work started, we hoped to write the definitive life

history of a typical granule. We now know that this is not possible. The evolution of a granule is strongly influenced by its environment, namely, by magnetic fields in its vicinity and by its location with respect to meso- and supergranular flows. Many, if not most, granules do not evolve to completion but rather are ended, probably randomly, by the radial expansion of another granule in their vicinity.

Small granules or fragments are another problem. Is there an objective way to handle them? Is there a size spectrum, perhaps turbulent, of small granules? Are the small granules the result of turbulent breakup of larger ones? Clearly, some smaller fragments are generated during the final stages of the exploding granule process. Are other small granules the signature of a turbulent convective layer? Are some just small convective cells? Here again we are tempted to make suggestions, but will await the results of new studies.

Finally, we reemphasize the importance of the digital movie techniques for studying and guiding data processing of images of granulation or any complex evolving system. Raw movies are so chaotic at high resolution as to be nearly incomprehensible. The three-dimensional Fourier filtering allows us to concentrate on any phenomenon of interest which can be isolated in the (k, ω)-plane. The all-pervading nature of exploding granules becomes evident only when the oscillations are removed, and the differences between quiet and magnetic granulation also become clearer. The ability to overlay the flow arrows and divergence maps on movie sequences was crucial to understanding the role of these flows. The eye-brain system is also very sensitive to time evolution and motion, when it is the relatively narrow range the system expects, so that it is critical to view movies at the proper "brain speed," both in forward and reverse order. Hopefully, the next few years will see the development of image-processing procedures that measure more accurately what we can see. Until that time, we can only comment that it is indeed unfortunate that journals cannot publish movies.

Special thanks are extended to the crew of Spacelab 2 and the controllers and planners on the ground who worked so hard to get these observations. Data reduction and analysis at Lockheed was assisted by Zoe Frank, Mike Levay, Michael Morrill, and Karen Chen. We would also like to acknowledge the ground-based observers around the world who supported both the US Naval Research Laboratory High Resolution Telescope Spectrograph and the SOUP experiment during the flight of Spacelab 2. We benefited from useful discussions with Juri Toomre, Goran Scharmer, Ake Nordlund, Aad van Ballegooijen, and Peter Brandt. And special thanks go to Hal Zirin of Big Bear Solar Observatory and Jack Harvey at the National Solar Observatory for providing magnetograms. The SOUP instrument development and data analysis were supported by the National Aeronautics and Space Administration under contract NAS8-32805. The CCD camera used to digitize all SOUP data was developed under contract NAS5-26813 for the Coordinated Instrument Package of the *Orbiting Solar Laboratory* (formerly known as the *High Resolution Solar Observatory*). The image processing systems for movie data analysis using laser optical disks have been supported by Lockheed Independent Research funds.

REFERENCES

Allen, M. S., and Musman, S. 1973, *Solar Phys.*, **32**, 311.
Bahng, J., and Schwarzschild, M. 1962, *Ap. J.*, **134**, 312.
Beckers, J. M. 1981, in *The Sun as a Star*, ed. Stuart Jordan (NASA SP-450), p. 11.
Beckers, J. M., and Canfield, R. C. 1975, in *Physiques des Mouvements dans les Atmosphères Stellaires*, ed. R. Cayrel and M. Steinberg (Colloques Internationaux du CNRS; Paris: CNRS), p. 219.
Bonet, J. A., Marquez, T., Roca-Cortez, T., Vazquez, M., Wohl, H., and Wittmann, A. 1984, in *Proc. NSO Conf. on Small Scale Dynamical Processes in Quiet Stellar Atmospheres*, ed. S. Keil (Sunspot, NM: NSO/AURA), p. 323.
Brandt, P. N., Scharmer, G. B., Ferguson, S., Shine, R. A., Tarbell, T. D., and Title, A. M. 1988, *Nature*, in press.
Bray, R. J., Loughhead, R. E., and Durrant, C. J. 1984, *The Solar Granulation* (Cambridge: Cambridge University Press).
Carlier, A., Chauveau, R., Hugon, M., and Rosch, J. 1968, *C.R. Acad. Sci. Paris*, **226**, 199.
Cox, A. 1988, *Ap. J.*, submitted.
Dialetis, C., and Macris, C. 1984, in *High Resolution in Solar Physics*, ed. R. Muller (Berlin: Springer), p. 164.
Dravins, D., Lindegren, L., and Nordlund, A. 1981, *Astr. Ap.*, **96**, 345.
Dunn, R. B., and Zirker, J. B. 1973, *Solar Phys.*, **33**, 281.
Hurlburt, N. E., Toomre, J., and Massaguer, J. M. 1984, *Ap. J.*, **282**, 557.
———. 1986, *Ap. J.*, **311**, 563.
Janssen, J. 1896, *Ann. Obs. Astr. Phys.*, **1**, 91.
Karpinsky, N. 1980, *Soln. Dannye*, **7**, 94.
Kawaguchi, I. 1980, *Solar Phys.*, **65**, 207.
Kitai, R., and Kawaguchi, I. 1979, *Solar Phys.*, **64**, 3.
Leighton, R. B. 1962, *Ann. Rev. Astr. Ap.*, **1**, 19.
Livingston, W. 1984, in *Proc. NSO Conf. on Small Scale Dynamical Processes in Quiet Stellar Atmospheres*, ed. S. Keil (Sunspot, NM: NSO/AURA), p. 330.
Macris, C. J. 1951, *Observatory*, **75**, 122.
Macris, C. J., and Rosch, J. 1983, *C.R. Acad. Sci. Paris*, **296**, 268.
Mehltretter, J. P. 1978, *Astr. Ap.*, **62**, 311.
Musman, S. 1972, *Solar Phys.*, **26**, 290.
Namba, O. 1986, *Astr. Ap.*, **161**, 31.
Namba, O., and Diemel, W. E. 1969, *Solar Phys.*, **26**, 290.
Namba, O., and van Rijsbergen, R. 1977, in *IAU Colloquium 38, Problems of Stellar Convection*, ed. E. A. Spiegel and J. P. Zahn (Berlin: Springer), p. 119.
Nordlund, A. 1984, in *Proc. NSO Conf. on Small Scale Dynamical Processes in Quiet Stellar Atmospheres*, ed. S. Keil (Sunspot, NM: NSO/AURA), p. 174
———. 1985, *Solar Phys.*, **100**, 209.
November, L., Simon, G., Tarbell, T., Title, A., and Ferguson, S. 1987, in *High Resolution Solar Physics II*, ed. G. Athay and D. Spicer (NASA CP-2483), p. 121.
Oda, A. 1984, *Solar Phys.*, **93**, 243.
Roudier, Th., and Muller, R. 1987, *Solar Phys.*, **107**, 11.
Schmidt, W., Knolker, M., and Schroter, E. H. 1981, *Solar Phys.*, **73**, 217.
Simon, G. W., Title, A. M., Tarbell, T. D., Topka, K. P., and the SOUP Team. 1988, *Ap. J.*, **327**, 964.
Steffen, M., Ludwig, H. G., and Kruss, A. 1988, *Astr. Ap.*, submitted.
Title, A., Tarbell, T., Simon, G., and the SOUP Team. 1986, *Adv. Space Res.*, **6**, 253.
Title, A. M., Tarbell, T. D., and the SOUP Team. 1987, in *High Resolution Solar Physics II*, ed. G. Athay and D. Spicer (NASA CP-2483), p. 55.
Wittmann, A. 1979, in *Small Scale Motions on the Sun* (*Mitt. Kiepenheuer-Inst.*, No. 179 [Freiburg]), p. 29.
Zahn, J.-P. 1987, in *Solar and Stellar Physics*, ed. E.-H. Schroter and M. Schussler (*Lecture Notes in Physics*, Vol. **292**), p. 55.

STUART FERGUSON, RICHARD SHINE, THEODORE TARBELL, ALAN TITLE, and KENNETH TOPKA: Lockheed Palo Alto Research Laboratory, Department 91-30, Building 256, 3251 Hanover Street, Palo Alto, CA 94304